Pontificia Universidad Católica del Perú

Facultad de Ciencias e Ingeniería

Búsqueda de Neutrinos pesados vía vértices desplazados en procesos de fusión de bosones vectoriales en colisionadores

TESIS PARA OPTAR EL TÍTULO PROFESIONAL DE LICENCIADO EN FÍSICA

Autor

Joaquin Aurelio Masias Teves

Asesor

Joel Jones Pérez

Lima, Agosto 29, 2019

ET LUX IN TENEBRIS LUCET
MCMXVII

Este trabajo está dedicado a la familia de mi hermana, y a su primera hija que está pronta a nacer.

Agradecimientos

Quiero agradecer a mi asesor el Dr. Joel Jones por el aprendizaje, el tiempo otorgado y el apoyo que me ha brindado a lo largo de este proyecto.

Tambien quiero agradecer al grupo de altas energías en la PUCP y a mis compañeros y amigos.

Finalmente, agradezco a mi familia por apoyarme a lo largo de mi carrera.

Abstract

The Standard Model (SM) is the theory that describes elementary particles and their fundamental interactions. In the Standard Model neutrinos are massless particles. Nevertheless, this has been proven wrong by neutrino oscillation experiments. Neutrinos possess mass, but several orders of magnitude below those of the other SM fermions. This invites the consideration of new physics, beyond that described by the SM, that could explain the smallness of neutrino mass. This is achieved, in particular, in the Type-1 Seesaw model, which is the focus of this work. Neutrinos are especially difficult to detect in colliders, since they are chargeless, they leave no tracks, and no energy in the calorimeters. However, if massive enough, these new neutrinos can decay into charged particles inside the collider, which results in tracks with displaced vertices. A complete analysis of this processes is required in order to characterize the parameters of these new particles. In this work we use the MonteCarlo simulation program MadGraph to study the relevant processes that involve these neutrinos. The principal objective of this work is to define the probability to observe the heavy neutrinos as Higgs decay products in the LHC (and HL-LHC), when they have been produced via vector boson fusion (VBF) and are in the section of parameter space useful for displaced vertices.

List of Figures

List of Tables

Contents

1 Introduction

The Standard Model (SM) of particle physics classifies all known elementary particles and describes the fundamental forces that mediate their interactions. The SM includes twelve spin $\frac{1}{2}$ particles, or fermions, and four force mediator spin 1 particles, or gauge bosons. The fermions are divided in six quarks: up (u), down (d), charm (c), strange (s), top (t) and bottom (b); and six leptons: electron (e), muon (μ), tau (τ) and their respective neutrino (ν_e, ν_μ, ν_τ). The gauge bosons are photons (γ), $W^\pm$ and Z, and gluons (g), which mediate electromagnetic, weak, and strong forces, respectively. It also provides an explanation for the generation of particle mass, via the Brout-Englert-Higgs (BEH) mechanism, which requires the addition of a spin 0 particle, the Higgs boson (H) . Since its conception, the SM has proven to be a very successful theory, with many experimental predictions. Still, there is evidence for physics beyond the SM, which point at its incompleteness. For example, in the SM, neutrinos are massless neutral leptons, yet, experimental observations on neutrino oscillations show they are massive particles [1–3] albeit with masses six orders of magnitude below the mass of the electron, the lightest particle in the SM. The SM must then be revised in order to generate the minuscule neutrino masses. Possible corrections must explain the new observed physics, while maintaining

the many successes of the SM. We study the phenomenology of such a model in the context of the LHC, the possible channels by which it can be probed and its limitations. Namely, we study the Seesaw mechanism, which adds new heavy neutrinos to the SM. We implement a 3+3 neutrino model, with two almost degenerate heavy neutrinos, and a mostly decoupled third. Possible probes for this model are studied on the parameter space of neutrino mass (M_4) and squared mixing ($|U_{\mu 4}|^2$).

Following this introduction, the second chapter describes the theoretical framework behind the Seesaw mechanism, primary pillar of the model used in this work. Then, we present details regarding the phenomenology of this model. The next chapter contains the simulation details, and finally we present the results and conclusions.

2 Theoretical Framework

2.1 Seesaw Mechanism

In this study we used a Seesaw type I model [4–7]. This is one of the simplest extensions to the SM that provide neutrino mass generation [8]. In the SM, neutrinos are left-handed Weyl (massless) fermions ν_L. The Seesaw type I postulates the existence of N_s additional "sterile" neutrinos N_R, which are singlets

under the SM gauge symmetries. When these particles have masses around the EW scale, they are also referred to as Heavy Neutral Leptons (HNL).

The SM Lagrangian is modified by:

$$\Delta\mathscr{L} = -Y_\nu^{ai}\bar{L}_a N_{Ri} H - \frac{M_{Rij}}{2}\bar{N}_{Ri}N^c_{Rj} + h.c. \tag{1}$$

and the appropriate kinetic terms. Here, Y_ν^{ai} are Yukawa couplings and M_{Rij} is the right handed neutrino mass matrix. Notice that if $M_R = 0$, N_R becomes the right handed component of a Dirac neutrino. For this reason, the N_R are usually referred to as right-handed neutrinos. If $M_R \neq 0$, the N_R are Majorana particles. Majorana fermions are their own antiparticles and are defined by the condition:

$$\psi = \psi^c \tag{2}$$

That is, a Majorana fermion is equal to its charge conjugate. Here, $\psi^c \equiv \gamma^0 C\psi^*$ is the charge conjugate of ψ, where C is the Charge conjugation matrix.

The Seesaw mechanism is best explained in a reduced scenario with a single pair of neutrinos, ν_L and N_R. We will denote ν (N) as the light (heavy) neutrino, where the former is to be identified with the SM neutrino.

In the weak basis $[\nu_L^c \; N_R]$ the mass matrix $\mathscr{M}$ is non diagonal:

$$\mathscr{M} = \begin{bmatrix} 0 & m_D \\ m_D & M_R \end{bmatrix} \tag{3}$$

Here, m_D is the Dirac mass term, defined as $v\frac{Y_\nu}{\sqrt{2}}$, where v is the vacuum expectation value of the Higgs (vev). A non-zero $m_L\nu_L^c\nu_L$ term is forbidden by Electroweak gauge symmetry, M_R doesn't have this limitation since N_R is sterile. We can then introduce a rotation to the mass basis $[\nu \; N]$ where $\mathscr{M}$ is diagonal:

$$\tilde{\mathscr{M}} = \begin{bmatrix} m_\nu & 0 \\ 0 & M_N \end{bmatrix} \tag{4}$$

A simple eigenvalue equation brings m_ν and M_N, and assuming $m_D << M_R$:

$$\begin{aligned} m_\nu &\simeq \frac{-{m_D}^2}{M_R} \\ M_N &\simeq M_R + \frac{{m_D}^2}{M_R} \end{aligned} \tag{5}$$

The eigenvectors are

$$\begin{aligned} \nu &\simeq (\nu_L + {\nu_L}^c) - \frac{m_D}{M_R}(N_R + {N_R}^c) \\ N &\simeq (N_R + {N_R}^c) + \frac{m_D}{M_R}(\nu_L + {\nu_L}^c) \end{aligned} \tag{6}$$

The m_ν mass term suffers a very strong suppression from M_R. Thus, one can generate the tiny, observed neutrino masses by introducing these heavy N neutrinos. The term $\frac{m_D}{M_R}$ in both equations indicates that ν is almost completely active (i.e., it interacts via the weak force), whereas N is almost completely sterile. To get an idea of the required size of M_R, we can express it as:

$$M_R \simeq \frac{-{m_D}^2}{m_\nu} = \frac{-v^2 Y_\nu^2}{2m_\nu} \tag{7}$$

For $m_\nu \simeq 10^{-2}$ eV, $v = 246$ GeV, and $Y_\nu \in [10^{-11}; 10^{-1}]$, M_R can take values from 10^{-6} to 10^{12} GeV.

2.2 The Low Scale Seesaw

The model used in the following chapters is a 3+3 Seesaw type I ($\nu_1, \nu_2, \nu_3, N_4, N_5, N_6$), with heavy neutrino masses in the GeV scale. The model proposed introduces two degenerate right-handed massive neutrinos ($M_{4,5} \in [1, 50]$ GeV) and a third heavier neutrino ($M_6 = 100$ GeV) with negligible mixing to the

other states. This scenario will behave like an effective $3+2$ model [9], as the third heavy neutrino is decoupled from the theory.

The 6×6 mass matrix is diagonalized:

$$\mathscr{M}_\nu = U diag(m_1, m_2, m_3, M_4, M_5, M_6) U^\dagger \tag{8}$$

Here, $\mathscr{M}_\nu$ is on the basis that diagonalizes Y_e, and U is a unitary transformation that describes the mixing between neutrinos. The U matrix can be decomposed into four 3×3 blocks.

$$U = \begin{pmatrix} U_{al} & U_{ah} \\ U_{sl} & U_{sh} \end{pmatrix} \tag{9}$$

Each block can be parameterized as [10, 11]:

$$\begin{aligned} U_{al} &= U_{PMNS} H, & U_{ah} &= i U_{PMNS} H {m_l}^{1/2} R^\dagger {M_h}^{-1/2}, \\ U_{sl} &= i \bar{H} {M_h}^{-1/2} R {m_l}^{1/2}, & U_{sh} &= \bar{H} \end{aligned} \tag{10}$$

With,

$$\begin{aligned} H &= (I + {m_l}^{1/2} R^\dagger {M_h}^{-1} R {m_l}^{1/2})^{-1/2} \\ \bar{H} &= (I + {M_h}^{-1/2} R m_l R^\dagger {M_h}^{-1/2})^{-1/2} \end{aligned} \tag{11}$$

In the equations above U_{PMNS} is the observed 3×3 Unitary neutrino mixing matrix, which we recover in the limit $H = I$. The diagonal heavy (mostly sterile) neutrino matrix is denoted as:

$$M_h = diag(M_4, M_5, M_6) \tag{12}$$

The other three light (mostly active) massive neutrinos as:

$$m_l = diag(m_1, m_2, m_3) = diag(m_1, \sqrt{\Delta m^2_{sol} + m^2_1}, \sqrt{\Delta m^2_{atm} + m^2_1}) \tag{13}$$

Where we assume normal ordering of ν masses. Both are 3×3 matrices, and Δm^2_{sol} and Δm^2_{atm} are the observed light neutrino mass squared differences, by solar and atmospheric neutrino experiments, respectively.

We also have a complex orthogonal matrix R, which is parameterized as:

$$R = \begin{pmatrix} c_{45} & s_{45} & 0 \\ -s_{45} & c_{45} & 0 \\ 0 & 0 & 1 \end{pmatrix} \begin{pmatrix} c_{46} & 0 & s_{46} \\ 0 & 1 & 0 \\ -s_{46} & 0 & c_{46} \end{pmatrix} \begin{pmatrix} 1 & 0 & 0 \\ 0 & c_{56} & s_{56} \\ 0 & -s_{56} & c_{56} \end{pmatrix} \tag{14}$$

where s_{ij} and c_{ij} are the sines and cosines of a complex angle, θ_{ij} + iγ_{ij} . Thus, the only free parameters left in the neutrino mass matrix are the three θ_{ij}, γ_{ij} pairs, the heavy neutrino masses, and the two Majorana CP phases present in

U_{PMNS}. For this study we take particular interest in the case where only one γ_{ij} (in this case γ_{45}) is different from 0 and considerably large ($|\gamma_{ij}| \gtrsim 3$). R becomes:

$$R_{45}(\theta_{45}, \gamma_{45}) = \begin{pmatrix} c_{45} & s_{45} & 0 \\ -s_{45} & c_{45} & 0 \\ 0 & 0 & 1 \end{pmatrix} =$$

$$\begin{pmatrix} \cos(\theta_{45})\cosh(\gamma_{45}) - i\sin(\theta_{45})\sinh(\gamma_{45}) & \sin(\theta_{45})\cosh(\gamma_{45}) + i\cos(\theta_{45})\sinh(\gamma_{45}) & 0 \\ -\sin(\theta_{45})\cosh(\gamma_{45}) - i\cos(\theta_{45})\sinh(\gamma_{45}) & \cos(\theta_{45})\cosh(\gamma_{45}) - i\sin(\theta_{45})\sinh(\gamma_{45}) & 0 \\ 0 & 0 & 1 \end{pmatrix} \tag{15}$$

Then, for large γ_{45}, $|\sinh(\gamma_{45})| \approx \cosh(\gamma_{45})$, and θ_{45} behaves like and overall phase:

$$R_{45}(\theta_{45}, |\gamma_{45}| >> 0) = \begin{pmatrix} \cosh(\gamma_{45})e^{-iz_{45}\theta_{45}} & -z_{45}\cosh(\gamma_{45})e^{-iz_{45}\theta_{45}} & 0 \\ -z_{45}\cosh(\gamma_{45})e^{-iz_{45}\theta_{45}} & \cosh(\gamma_{45})e^{-iz_{45}\theta_{45}} & 0 \\ 0 & 0 & 1 \end{pmatrix} \tag{16}$$

Here z_{45} is the sign of γ_{45}. We also assume $H \sim I$. This lets us write the "active to heavy" elements of the mixing matrix U as:

$$U_{a4} = -iz_{45}(Z_a^{NO})^{45}\sqrt{\frac{m_2}{M_4}}\cosh(\gamma_{45})e^{-iz_{45}\theta_{45}} \tag{17}$$

$$U_{a5} = (Z_a^{NO})^{45}\sqrt{\frac{m_2}{M_5}}\cosh(\gamma_{45})e^{-iz_{45}\theta_{45}} \tag{18}$$

$$U_{a6} = (U_{PMNS})_{a3}\sqrt{\frac{m_3}{M_6}} \tag{19}$$

with:

$$(Z_a^{NO})^{45} = (U_{PMNS})_{a2} + iz_{45}\sqrt{\frac{m_1}{m_2}}(U_{PMNS})_{a1} \tag{20}$$

In the mass basis, the interaction terms of the Lagrangian can be expressed as [12]:

$$\mathscr{L}^{W^\pm} = -\frac{g_W}{\sqrt{2}}W_\mu^- \bar{l}_\alpha \gamma^\mu U_{\alpha i} P_L n_i + h.c. \tag{21}$$

$$\mathscr{L}^{Z} = -\frac{g_W}{4c_W}Z_\mu \bar{n}_i \gamma^\mu \left[C_{ij}P_L - C_{ij}^* P_R\right] n_j \tag{22}$$

$$\mathscr{L}^{h} = -\frac{g_W}{4M_W}h\bar{n}_i \left[C_{ij}\left(m_{n_i}P_L + m_{n_j}P_R\right) + C_{ij}^*\left(m_{n_i}P_R + m_{n_j}P_L\right)\right] n_j \tag{23}$$

Where C and m are 6×6 matrices defined as:

$$C_{ij} = \sum_{\alpha=1}^{3} U_{i\alpha}^\dagger U_{\alpha j}, \qquad m_n = \text{Diag}(m_{n_i}) = \text{Diag}(m_1, m_2, m_3, M_4, M_5, M_6) \tag{24}$$

We analyze a section of the parameter space defined by the following condi-

tions:

$$
\begin{aligned}
m_1 &= 10^{-2}\text{eV} \\
1\text{GeV} < M_4 &\approx M_5 < 50\text{GeV} \\
M_6 &= 100\text{GeV} \\
\gamma_{46} &= \gamma_{56} = 0 \\
5 < |\gamma_{45}| &< 10
\end{aligned}
\tag{25}
$$

For this choice of parameters, we find $10^{-7} < |U_{\mu 4}|^2 < 10^{-5}$, $|U_{a4}|^2 \approx |U_{a5}|^2$ and $|U_{a6}|^2 \approx 0$. In the latter term there is a very large suppression from M_6 and no $\cosh(\gamma_{45})$ enhancement. In conclusion, we have a parameterization that mixes light neutrinos to two, almost degenerate, heavy neutrinos; and to a third, albeit with a very suppressed probability.

For exact degeneracy, the two Majorana spinors can be combined into one massive Dirac neutrino.

This zone of the parameter space is testable with existing experiments, in this case the LHC, and the near-future HL-LHC. We implement the model in SARAH [13] and using SPheno [14, 15] we obtain the Branching ratios shown in Figure 1.

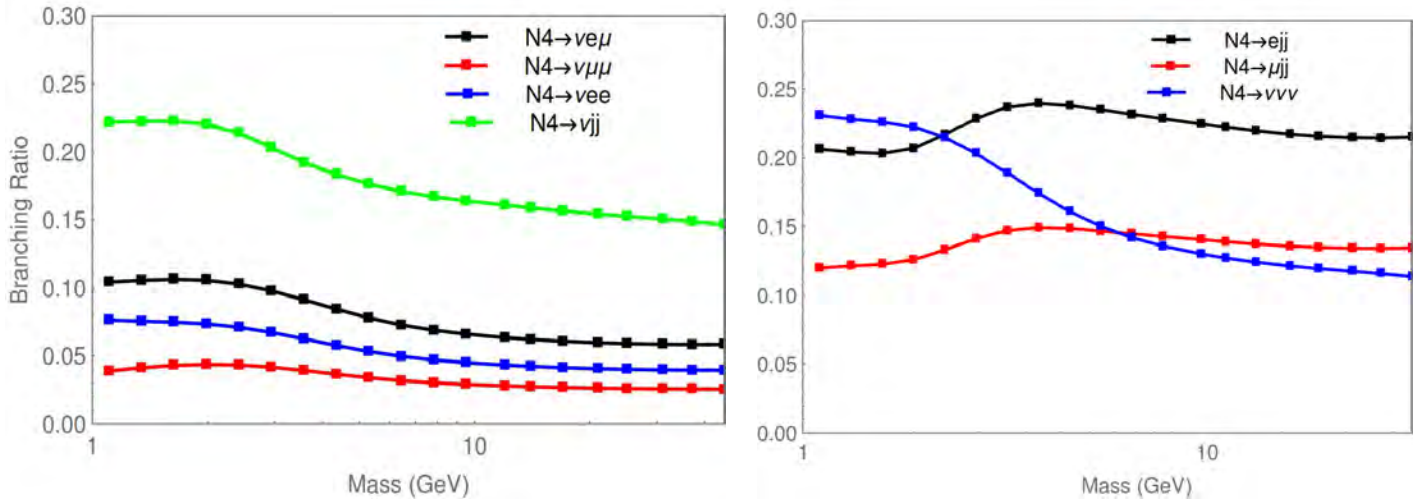

Figure 1: Branching Ratios for N_4 as a function of mass.

There is no mixing dependence in the BR because of cancellation between partial and total decay widths. Here e, μ, τ denote both particle and antiparticle, j denotes all possible jet constituents, and ν sums over the 3 light neutrinos. The relevant BR in this study are $N_4 \to \nu e\mu$, $N_4 \to \nu jj$, $N_4 \to \nu ee$, $N_4 \to ejj$ and $N_4 \to \nu\mu\mu$. These processes represent between 40% and 50% of all N_4 decays. Other processes, of the form $N_4 \to ljj$,$N_4 \to \nu\nu\nu$ with relevant BR are also shown. Processes containing tau leptons or b-jets are not studied in this work, and for low N_4 mass they have negligible contributions.

3 Vector Boson Fusion and Displaced Vertices

3.1 The LHC

The Large Hadron Collider (LHC) is the largest particle collider in the world, built by the European Organization for Nuclear Research (CERN). Its main purpose has been to probe the SM, where it has thoroughly succeeded by discovering many previously unseen predicted particles, such and exotic baryon states, and most importantly the Higgs boson [16] [17]. It has also tested predictions in order to address some of the unsolved questions in physics, such as the existence of supersymmetric particles, the matter/antimatter asymmetry and weakly interacting dark matter.

The four main experiments at LHC are ATLAS, CMS, LHC-b and ALICE. In these experiments protons collide at very high energies ($\sqrt{s} = 13$ TeV) and produce an enormous amount of particles. Then, the data of the collision is processed and only a sample is stored, since the sheer amount of data is too large to collect. The LHC detectors have trigger systems to select the data to be stored. A hardware trigger, involving physical effects on the detectors, is called a level one trigger. Software triggers are level two. If an event does not set off a trigger it is lost forever.

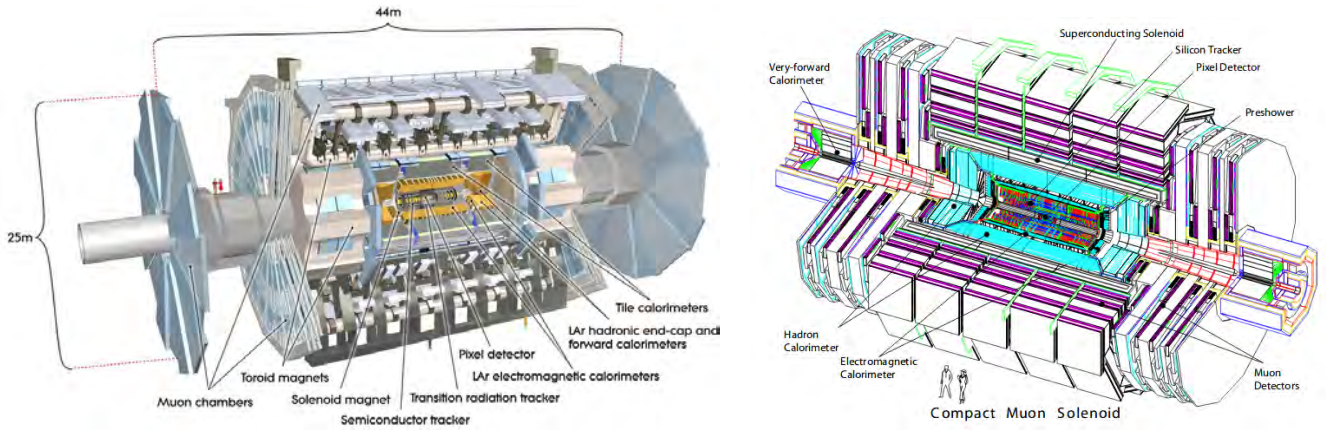

Figure 2: ATLAS and CMS experiments.
Taken from: ATLAS Collaboration (2008). The ATLAS Experiment at the CERN Large Hadron Collider. IOP Publishing. doi:10.1088/1748-0221/3/08/s08003 & CMS Collaboration (2008). The CMS Experiment at the CERN Large Hadron Collider. IOP Publishing. doi:10.1088/1748-0221/3/08/s08004

In the context of colliders, cross section is measured in barns (b) : 1b$=10^{-28}$ m^2 . Inelastic proton-proton collision cross section σ_{pp} is at the tens of milibarns level, with little energy dependence [18]. Protons are grouped in bunches of 10^{11} protons, which move at nearly the speed of light, and collide at 40 MHz. The beam line has a transverse area $\sigma_{beam} = 10(\mu\text{m})^2$, and the rate of collisions can be calculated as:

$$Rate_{\text{events}} = \left(10^{11}\frac{\text{protons}}{\text{bunch}}\right)^2 \times \frac{10\text{mb}}{(10\mu\text{m})^2} \times 40\ \text{MHz} \tag{26}$$

This gives a total of 4×10^9 collisions per second. The collision rate is measured in terms of the luminosity. Instantaneous luminosity times the cross section gives the rate of events, whereas integrated luminosity times cross section gives the total events per run.

It is convenient to analyze the data in terms of the most accessible, Lorentz

invariant quantities. Four-momentum (E, p_x, p_y, p_z) can be related between CM and Lab frames via a boost along the beam line, which is set along the z axis. Then, the p_x and p_y components are invariant between systems, as well as the azimuthal angle $\phi = \arctan\frac{p_x}{p_y}$, and the $\vec{p_T} = (p_x, p_y)$. The longitudinal momentum of a particle p_z and its total energy E are not easy to reconstruct, since information can be lost along the main axis, nor are they invariant between frames.

One can define the rapidity: $y = \frac{1}{2}\ln\frac{E + p_z}{E - p_z}$. The difference in rapidity is Lorentz invariant, which motivates the definition of ΔR as an invariant measure of angular displacement:$\Delta R_{ab} = \sqrt{(y_a - y_b)^2 + (\phi_a - \phi_b)^2}$. If the particles are massless (which they are at very good approximation), y reduces to the pseudo rapidity η = ln cot $\frac{\theta}{2}$, where θ is the zenith angle.

Some particles can pass freely through the detectors. A part of their information can be reconstructed from the difference of initial and final total transverse momentum, this is defined as $\vec{p}_T^{miss} = -(\sum \vec{p}_T)^{visible}$. The modulus of $\vec{p}_T^{miss}$ is sometimes called "missing transverse energy". For example, neutrinos leave the detector without interacting, but still take momentum with them. Another useful quantity is the invariant mass of a particle system, defined as:

$$m_{\text{system}} = \left| \sum_{\text{constituents j}} p_j^{\mu} \right|^2 \tag{27}$$

This can be used to reconstruct the mass of the parent particle in the case of on-shell decays. These quantities allow to establish triggers and cuts over the data, in order to pinpoint specific events and processes.

The CMS (Compact Muon Solenoid) and ATLAS (A Toroidal LHC ApparatuS) experiments (Fig. 2) are considered in this study. Both detectors consist of the same basic design: an inner tracker near the beam line to measure tracks of charged particles, an electromagnetic calorimeter (ECAL) which measures and ”absorbs” the energy of electrons and photons, a hadronic calorimeter (HCAL) which measures the energies of neutrons and protons, and at the outside a muon detector, which measures the energy of muons through their curvature in an strong magnetic field. These experiments have differences in the specifications of their parts, which are not of much importance in a phenomenological study.

3.2 Vector Boson Fusion

In general, searches for heavy neutrinos use an outgoing charged lepton as a trigger in processes that involve W bosons (Fig. 4). These leptonic channels are considerably clean and have large cross-sections, even if heavy cuts are imposed on the outgoing lepton. However, this search can only probe the heavy neutrino couplings with the W boson, couplings with H and Z have an outgoing light neutrino.

A particularly interesting process for the study of neutrino couplings to neutral bosons is via Vector Boson Fusion (VBF) (Fig. 3) [19]. The colliding protons "radiate" a weak boson pair which then "annihilates" into the Higgs or a Z. In this study, since neutrinos are chargeless, the only way to trigger is via the VBF topology. This will most likely not represent a discovery channel, but will be relevant for the understanding of the heavy neutrino properties. The cuts required for a VBF trigger are presented in Chapter 4. Similar searches in the context of VBF phenomenology have been made, for new Neutral Gauge Bosons [20] and HNL in the TeV scale [21].

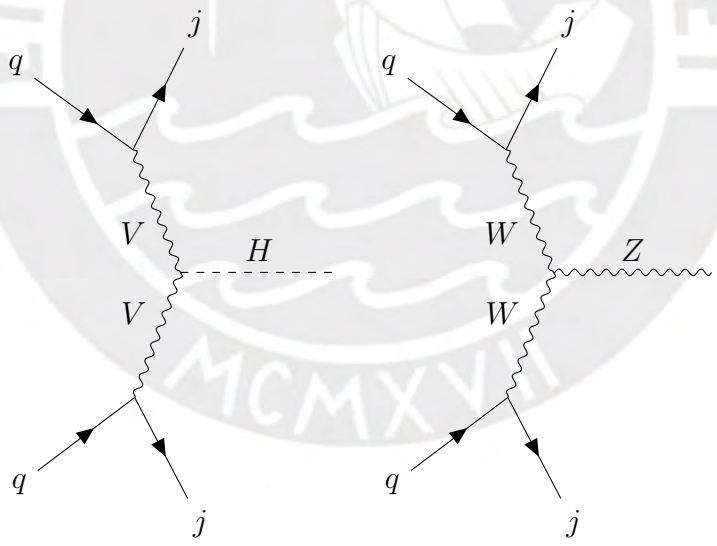

Figure 3: Feynman Diagrams for Vector Boson Fusion. V denotes Weak Gauge Bosons (W or Z).

As and example, we use MadGraph to reproduce the VBF Higgs cross section as a function of the Higgs mass (Fig. 5). At $m_H = 125$ GeV the cross section sits around 5 pb, while VBF Z boson production is around 95 pb. The VBF

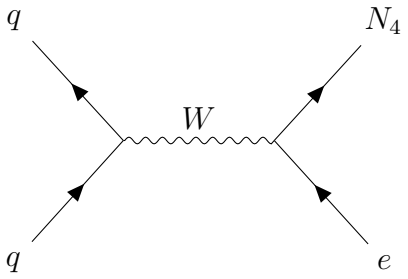

Figure 4: Pure leptonic channel for N_4 production, via off-shell W boson.

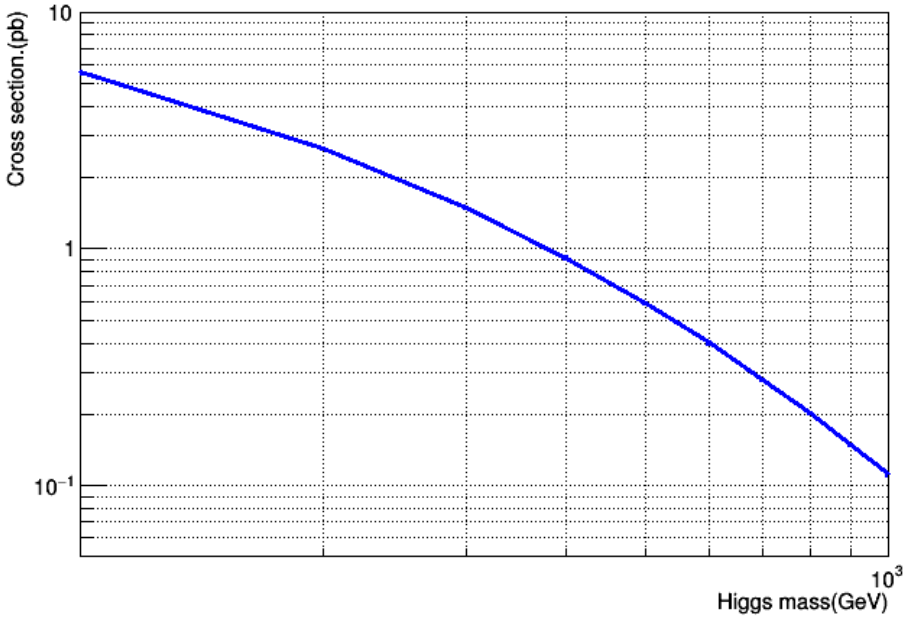

Figure 5: VBF Higgs cross section as a function of it's mass

diagram topology suggests cuts on the outgoing jets, and on the decay products of the Higgs and Z bosons. This can be used to tag the VBF and isolate it from other processes, and also acts as trigger. . In particular, we are interested in the case where the Higgs (or Z) decays to $N_4\ \nu_i$ Fig. 6 (or similarly $N_5\ \nu_i$). Notice that in this model, the Higgs cannot be distinguished from a Z boson, this can be subject of further study [22].

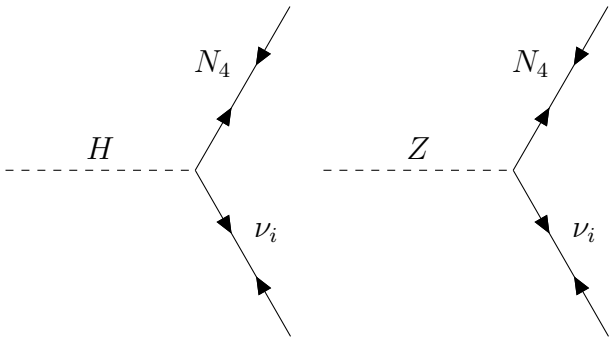

Figure 6: Vertex for Higgs (Z) decay into Majorana neutrino.

3.3 Displaced Vertices

From the perspective of collider physics, an interesting case is in the region of parameter space for which the heavy neutrinos (HN) are long lived particles (LLP) that can decay within the LHC detectors. The posterior decay produces a second, displaced vertex (DV). This would be a distinctive signature of their existence, as it has a negligible irreducible background from SM processes. Recently, several studies have pushed for this kind of dedicated LHC searches for heavy neutrinos with associated charged leptons from Higgs decays [23] [24].

The heavy neutrino decay width at rest Γ_{N_4} is calculated from the model via SPheno 4.0.3 for each point in the parameter space. An approximate measure of the distance it travels in the detector before decaying can be computed as $L_{N_4} = \frac{\hbar c}{\Gamma_{N_4}}$. (Fig. 7). If the HN has a decay length less than 1mm, the resolution is insufficient to distinguish the DV from the primary vertex (PV), and it is said that it decays promptly. If it has a decay length greater than 1 m, it decays

outside the tracker. Similarly, we obtain the decay time on its rest frame as $\tau_{N_4} = \dfrac{\hbar}{\Gamma_{N_4}}$.

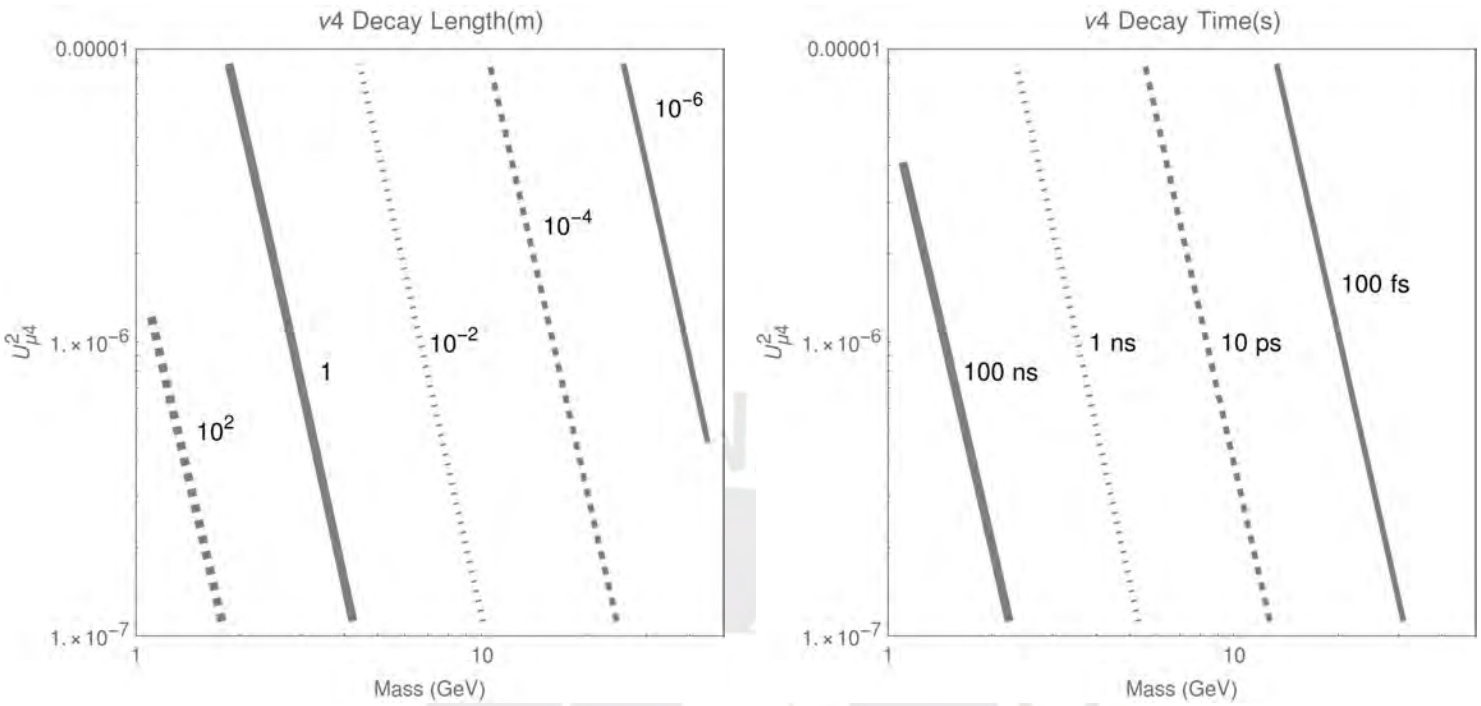

Figure 7: Left:Simplified Decay Length (m) $L_{N_4} = \dfrac{\hbar c}{\Gamma_{N_4}}$. Right: Rest frame Decay Time (ns) $\tau_{N_4} = \dfrac{\hbar}{\Gamma_{N_4}}$.

4 Simulation

MadGraph5_aMC@NLO is a framework for Monte Carlo event generation [25]. Its main purpose is the simulation of SM and BSM processes. It provides elements necessary for high-energy phenomenology, such as the computations of cross sections (at Leading Order (LO), Next to Leading Order (NLO) and including loop corrections), the generation of hard events and their matching with event generators, and the use of a variety of tools relevant to event manipulation and analysis. The software can be used in conjuction with sev-

eral other programs such as Pythia8 [26, 27], used for parton showering and hadronization. This allows for a thorough simulation of the present and future experiments at the LHC.

The Les Houches card for SPheno is generated in Mathematica (ver. 11.0.1.0) with SARAH package SSP (ver.1.2.5) [28]. The parameter card for the See-saw Model is generated with SPheno 4.0.3., this is then used as input for MadGraph5_AMC@NLO (ver. 2.6.4). Events are generated with $\sqrt{s} = 13$ TeV. In our analysis b quark pdf's are included at the primary vertex, since they have considerable contributions to VBF Higgs production. Cross sections are calculated at tree level. The hadronization and showers are made via Pythia8.2, of which, the output is given in HEPMC format at truth level (the analysis is discussed in Appendix A). The consideration of reconstruction efficiencies is left as further work [22]. We scanned M_4 from 1 GeV to 50 GeV, with squared mixings $|U_{\mu 4}|^2$ from 10^{-7} to 10^{-5} (20 samples for each,logarithmically scaled). Finally, the data analysis is done with the combined use of Root and Mathematica.

4.1 Event Selection and Triggers

Previous studies in BSM phenomenology at the LHC have analyzed possible cuts for the search of new physics [29], similarly, we present the cuts used for HN searches. The VBF topology is characterized by two high p_T forward jets (j_1, j_2), with large a pseudorapidity gap, located in opposite hemispheres of the detector, and TeV scale invariant masses [19]. This topology is particularly useful in reducing QCD multijet backgrounds, thus, we use it as a first event selection criterion. The criteria are presented in Table 1. Here, $lead$ and $sub-lead$ refer to the two most energetic jets. These are experimental requirements, imposed over the reconstructed objects.

VBF Selections	
$p_T^{lead}(jet)$	>30 GeV
$\lvert\eta^{lead}(jet)\rvert$	< 5.0
$p_T^{sub-lead}(jet)$	>30 GeV
$\lvert\eta^{sub-lead}(jet)\rvert$	< 5.0
$\eta(jet1)\cdot\eta(jet2)$	<0
$\lvert\Delta\eta(j_1,j_2)\rvert$	>4.2
$m_{j_1 j_2}$	>750 GeV

Table 1: Table displaying VBF and DV selection criteria.

The different decay modes of the heavy neutrino lead to different experimental signatures. We focus on:

- Displaced Dilepton (μe) searches [30, 31]
- Lepton jet ($\mu^-\mu^+$&e^-e^+) searches [32–34]

- Displaced jet searches [35, 36]

4.1.1 Displaced Dilepton Searches

Displaced Dileptons refer to a muon-electron pair, that is produced via de de-cay of a LLP. Heavy Neutrino can disintegrate via the Lepton Flavor Violating (LFV) decay $N_4 \rightarrow \nu_i\ e^{\pm}\mu^{\mp}$(Fig. 8). This motivates a search for displaced dilepton production in CMS. The heavy neutrino is required to decay within the tracker, $\sqrt{L_x^2 + L_y^2} < 40\text{mm}$ & $L_z < 300\text{mm}$, where L_x, L_y, L_z are the distances in x, y, z travelled by the heavy neutrino before decaying.

The specific cuts for this channel are shown in Table 2. The search requires high-p_T leptons, with low pseudorapidity, opposite charges and considerable angular separation. In this case, the discriminating kinematical variable is the impact parameter:

$$d_0^l = \frac{|p_x^l L_y - p_y^l L_x|}{p_T^l} \tag{28}$$

It is defined as the distance of closest approach to the beamline. Here, p_T^l is the p_T of each lepton and $p_{x,y}^l$ are the x and y components of the lepton momentum.

The 13 TeV CMS analysis then defines three non-overlapping signal regions (SR):

- **SR III**: $|d_0|_{e,\mu} > 1000\mu m$

Criterion	$\mu - e$	
Central Selections		
Particle	μ	e
p_T	> 40 GeV	>42 GeV
$\|\eta\|$	< 2.4	< 2.4
$\Delta R(\mu,e)$	>0.5	

Table 2: Table displaying cuts for a displaced dilepton search.

- **SR II**: $|d_0|_{e,\mu} > 500\mu m$ & at least one of the leptons outside of **SR III**.
- **SR I**: $|d_0|_{e,\mu} > 200\mu m$ & at least one of the leptons outside of **SR III** & **SR II**.

The search over this regions greatly reduces the SM background. An individual analysis for each SR is presented in Chapter 5.

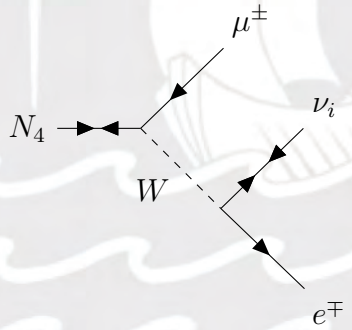

Figure 8: Heavy Neutrino decay into light neutrino and a muon electron pair.

4.1.2 Lepton Jets

Lepton jets are defined as leptons and/or jets (pions) within a cone $\Delta R = \sqrt{\Delta\phi^2 + \Delta\eta^2} < 0.5$. Depending on their constituents they can be classified as 3 types:

- Type 0: At least two muons and no jets found within the ΔR cone.

- Type 1: At least two muons and one jet or electron found within the ΔR cone.
- Type 2: At least two electrons or jets and no muons found within the ΔR cone.

For this study the cases of interest are of Type 0 (μ lepton jet) and Type 2 (e, π lepton jet). The cuts used are shown in Table 2. The relevant Feynman diagram topology is displayed in Fig. 9.

Criterion	μ lepton jet	e lepton jet
Central Selections		
$p_T(leptonjet)$	>20 GeV	>20 GeV
$\lvert\eta(\mu/e)\rvert$	< 2.4-(1.0; 1.1)	< 2.4-(1.0; 1.6)
$\Delta R(\mu_1/e_1, \mu_2/e_2)$	< 0.5	<0.5
$\lvert z_o\rvert$	< 280mm	-
Jet Width	-	< 0.058

Table 3: Table displaying cuts for Type 0 and Type 2 lepton jet searches.

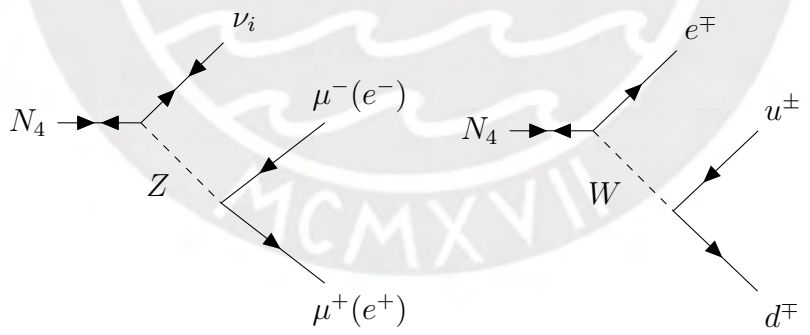

Figure 9: Right: Heavy Neutrino decay into light neutrino and a lepton anti-lepton pair. Left: Heavy Neutrino decay into electron and a pair of jets (pion).

The lepton jet is constructed from the total momentum of its constituents, which are required to be within ΔR < 0.5 of each other. It must pass the standard jets selections, that is p_T > 20 GeV and $|\eta|$ < 2.4 (the excluded η ranges

are due to transition regions, and are therefore rejected). For Type 0 and Type 2 lepton jets there are then different criteria.

Type 0 require to be non-combined, that is, their direction can not be reconstructed to the primary vertex. It must not be associated to a track, this is achieved by having the HN decay outside the tracker both $\sqrt{L_x^2 + L_y^2} < 4$ m and $|L_z|$ 5.5 m and either($\sqrt{L_x^2 + L_y^2} > 1.05$ m or $|L_z| > 3$m. A requirement on the muon longitudinal impact parameter z_o, defined as the value of z of the point on the track that determines d_0 (i.e, the value of z when the particle is a distance d_0 from the beam axis), is also imposed ($|z_o| < 280$mm). There are 3 possible trigger regions for Type 0 events:

- Narrow scan: Requires a leading muon with p_T > 20 GeV, and subleading muon with p_T > 6 GeV
- Trimuon: At least 3 muons, each with p_T > 6 GeV
- CalRatio: A muon jet with p_T > 30 GeV and low EM fraction ($log(E_{HCAL}/E_{ECAL}) \geq 1.2$.This can be enforced by requiring that the HN decays inside the $HCAL$.

Only Narrow scan and CalRatio are accessible in this study.

Type 2 search imposes no requirement on the impact parameter.In turn, the search requires:

- Jet Width < 0.058: A discerning variable for jets defined as $W = \frac{\Sigma_i \Delta R^i \cdot p_T^i}{\Sigma_i p_T^i}$. It is the average distance of a jet constituent to the jet direction weighted with the energy of the constituent: It is related to the jet mass, but not as sensitive to detector effects.

- EM fraction < 0.1: Low energy deposits at the $ECAL$, HN decays inside the $HCAL$

Type 2 jets also require cuts on variables not accessible, or constructable, from the ATLAS Delphes card, namely: Jet Timing, Jet Vertex Tagger (JVT) and BIB(Beam induced background) tagging. This variables allow to discriminate whether the electron jet comes from a DV and reduce backgrounds.

4.1.3 Displaced Jets Searches

Standard jets originating outside the primary vertex (PV) are of particular interest as event selection criteria for the HN search (Fig. 10). We present two possible different searches, in CMS and ATLAS, respectively. Their kinematical cuts are summarized in Table 4.

Criterion	CMS	ATLAS
Central Selections		
p_T j_1,(j_2)	>30(30) GeV	>70(-)GeV ∨>25(25)GeV
$\|\eta\|$ j_1(j_2)	<1.48	< 4.9
DV Selections	No	Yes
p_T^{miss}	>120GeV	>200GeV
$N^{\#}$ tracks	-	>5
m_{DV}	-	>10 GeV

Table 4: Table displaying cuts for CMS and ATLAS displaced jet searches.

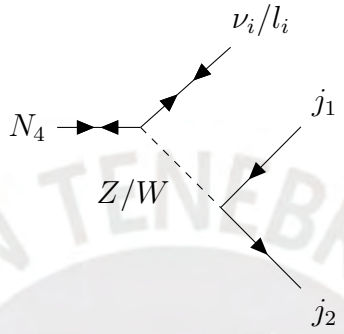

Figure 10: Heavy Neutrino decay into light neutrino and a muon electron pair.

- **CMS**

The displaced Jet search at CMS requires at least 2 jets with $p_T > 30$GeV, with considerably low pseudorapidity, $|\eta| < 1.48$; and high missing Energy trigger $p_T^{miss} > 120$ GeV. The CMS collaboration presents many calorimetry requirements for ”jet cleaning”, such as cuts on the minimum energy deposited in the electromagnetic (E_{CAL}) and hadronic calorimeters (H_{CAL}), and the time of the jet's detection (t_{jet}). The jet displacement is determined by requiring a delayed detection of the jets $t_{jet} > 3$ ns. Their specifications can be found in [35]. This cut criteria can be imposed on Geant4, via a simulation of the CMS detector, which is not open source.

- **ATLAS**

The ATLAS search requires at least 2 jets, and considers two scenarios. At least one jet with $p_T > 70$ GeV, or 2 jets with $p_T > 25$ GeV. It imposes no pseudorapidity requirements other than the detector's limitations, $|\eta|$<4.9. The search has a very high missing Energy trigger $p_T^{miss} > 200$ GeV, and in contrast to the CMS search, the DV selection criteria must be included.

- The vertex position must be within the fiducial volume of the tracker, $\sqrt{L_x^2 + L_y^2} < 300$ mm and $|L_z| < 300$ mm.
- Transverse distance between the interaction point and the decay position $\sqrt{L_x^2 + L_y^2} > 4$ mm.
- The DV must have at least 5 associated tracks, which must be charged and stable, with $p_T > 1$ GeV and $|d_0| > 2$ mm.
- The DV must have reconstructed invariant mass $m_{DV} > 10$ GeV.

5 Results

We present the cross section for heavy neutrino (N_4) production via the decay of a VBF Higgs or Z boson (Fig. 11). The Z contributions are dominant for $M_4 \simeq 1 - 10$ GeV and its dependence on the M_4 mass is only kinematical. The

results can be written in the form $\sigma(pp \to H(Z)jj)_{VBF} \times BR(H(Z) \to \nu_i N_4)$. The branching ratios are considerably low, between $\sim 10^{-9}$ - 10^{-3}, which is expected from this model. As a benchmark, we calculate the integrated Luminosity needed to generate 100 events (Fig. 12). The scenario nearest to present experiments requires $L \simeq 10^3$ fb^{-1}, an order of magnitude above current integrated luminosity at the LHC, at the scale of the HL-LHC. Within the evaluated parameter space, the expected heavy neutrino events at the LHC ($L = 300$ fb^{-1}) (Fig. 13) go up to at most two hundred events. The HL-LHC has expected Luminosity $L = 3000$ fb^{-1}, which adds an order of magnitude to the number of events. Final results must be multiplied by a factor of two since $M_4 \simeq M_5$.

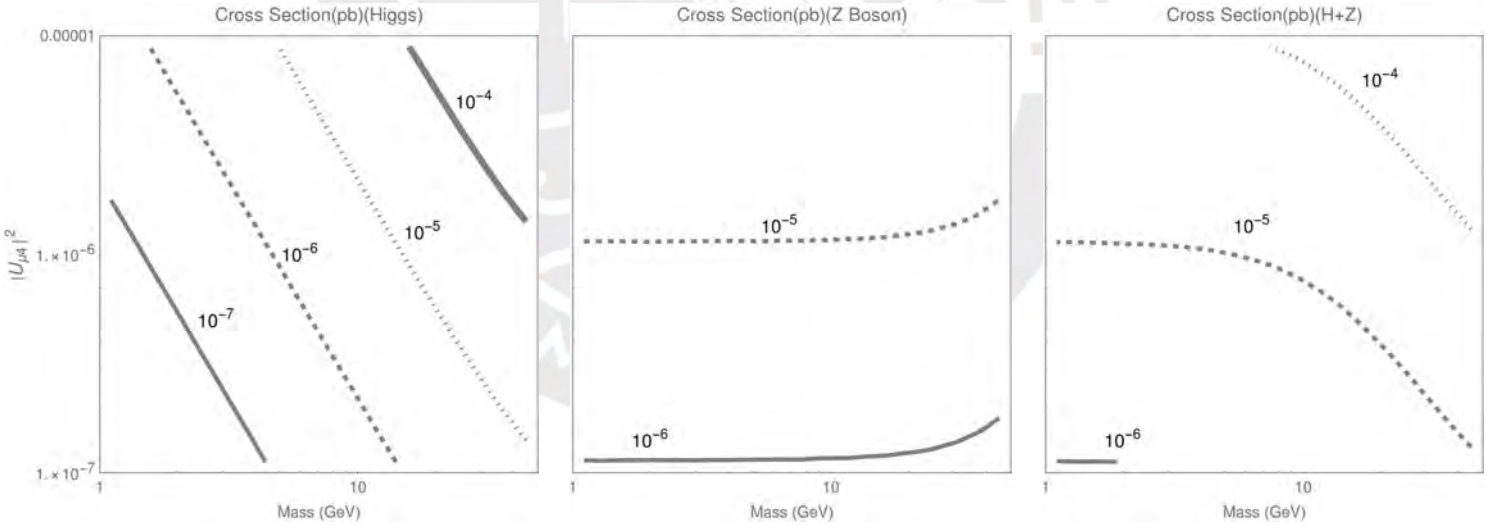

Figure 11: Left: Cross Section (pb) for $pp \to Hjj, H \to \nu_i N_4$. Middle: Cross Section (pb) for $pp \to Zjj, Z \to \nu_i N_4$. Right: Sum of both contributions.

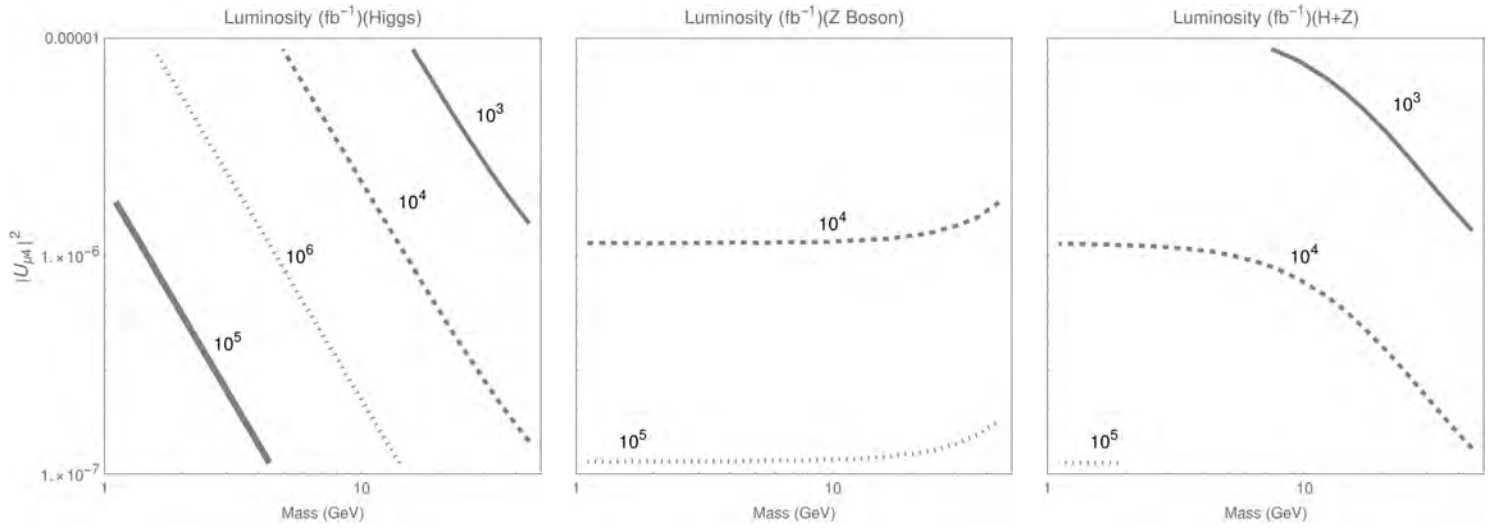

Figure 12: Luminosity (fb^{-1}) needed for 100 events in N_4 production via VBF and decay of: Right: Higgs, Middle: Z bosons and Left: Both.

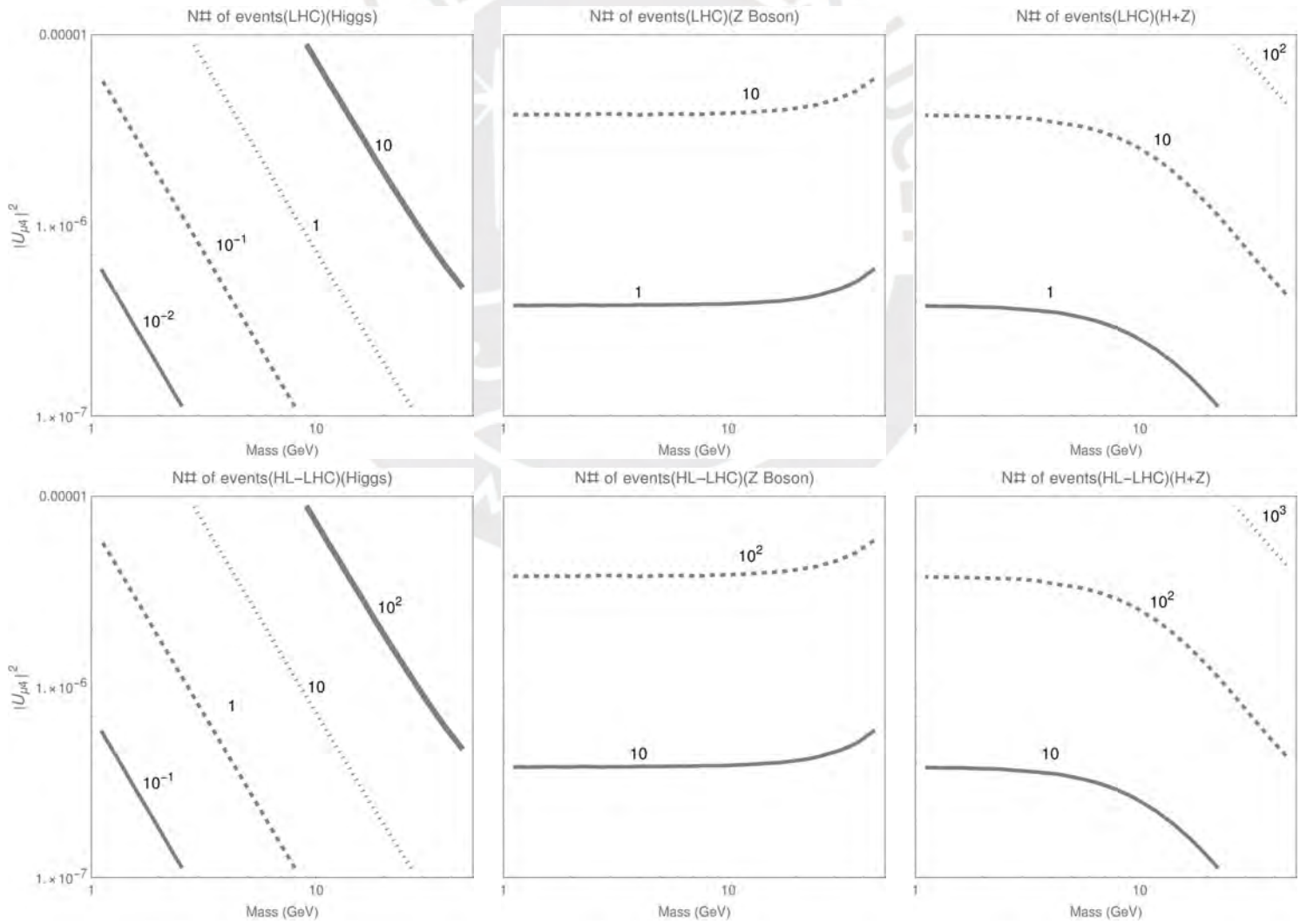

Figure 13: Expected number of events at present LHC (300 fb^{-1}), top row and future HL-LHC (3000 fb^{-1}), bottom row for N_4 production via the decay of: Right: Higgs, Middle: Z bosons and Left: Both.

We now present the results for the different detection channels discussed in chapter 4:

5.1 Displaced Lepton Searches

We search for lepton pairs ($e\mu$) in agreement with the cuts described in Chapter 4. We generate, via MadEvent, 10000 $pp \to H(Z)jj$, $H(Z) \to \nu_i N_4$, $N_4 \to \nu_i \mu^{\pm} e^{\mp}$ events. Our benchmark scenario: M_4= 14 GeV, $|U_{\mu 4}|^2$= 10^{-6} has Higgs and Z boson contributions of the same order. The kinematics of the leptons for the benchmark scenario show low p_T and $|\eta|$ distributions (Fig. 14), and considerably small ΔR distances and impact parameters (Fig. 15). The trigger cuts are most stringent in the p_T and ΔR requirements, as seen in Table 5. The required leptons must have considerable transverse momentum and not be collimated, which is not expected, since high p_T leptons require a boosted N_4 decay, which in turn makes them collimated. Given these two cuts, the number of events that survive in the DV-relevant part of the parameter space is 98 of 10000 in a best case scenario. The number of events on this benchmark is further constrained by the individual SR searches, with 0, 2, and 15 events for signal regions III, II and I, respectively. A total of 17 events, which is roughly equivalent to $10^{-4}(10^{-3})$ detections per LHC(HL-LHC) run. Thus, individual SR searches are impossible with such a low number of events.

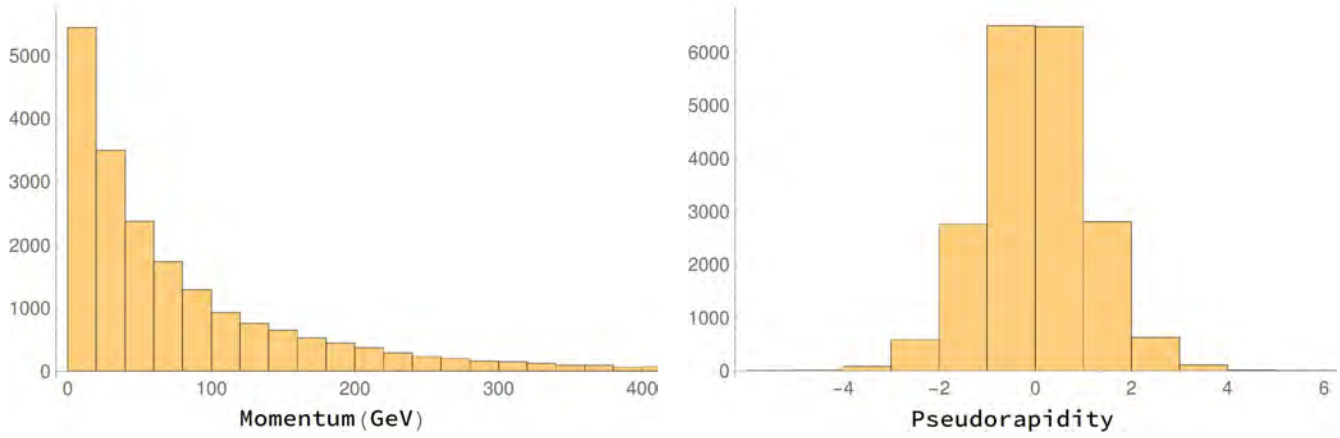

Figure 14: Left: Total p_T distribution for final state leptons. Right:$|\eta|$ distribution for final state lepton.

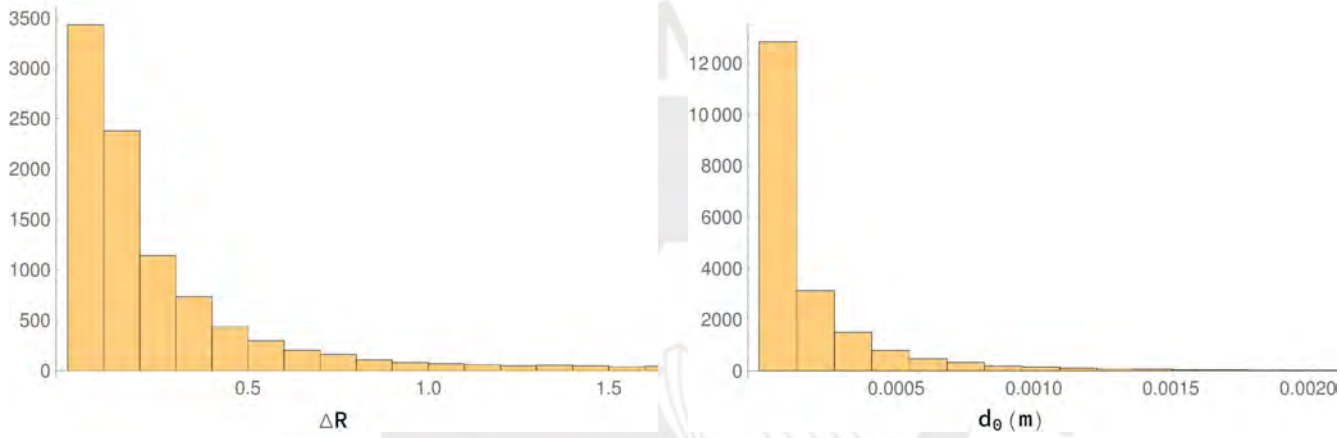

Figure 15: Left:$\Delta R_{\mu e}$ distribution for final state leptons. Right:d_0 distribution for final state leptons

5.2 Lepton Jet Searches

- Type 0 $(\mu^-\mu^+)search$

  Similarly to dilepton search, we follow the cuts described in Chapter 4. We generate, 10000 $pp \to H(Z)jj, H(Z) \to \nu_i N_4, N_4 \to \nu_i \mu^+\mu^-$ events. The squared mixing is fixed ($|U_{\mu 4}|^2$= 10^{-6}), and we analyze how the kinematics change for several neutrino masses. In Table 6 we display the number of surviving events (out of 10000) for the selection cuts, and for the 2 analyzed trigger regions. These are overlapping signal regions so we also present the

Cut Flow ($\mu - e$)		
Criterion	Individual	Combined
$\sqrt{L_x^2 + L_y^2} < 0.04$m	9968	9968
$\lvert L_z \rvert < 0.3$m	10000	9968
$\lvert\eta(e)\rvert < 2.4$	9264	9231
$\lvert\eta(\mu)\rvert < 2.4$	9266	9020
$p_T(e) > 42GeV$	5828	5481
$p_T(\mu) > 40GeV$	5880	3707
$\Delta R_{\mu e} > 0.5$	3294	98

Table 5: Table displaying individual and combined cuts for displaced dilepton search simulation. Ten thousand initial events.

overlap and the final surviving events. Higgs and Z boson contributions are both considered, and in this range the Z boson VBF cross-section is an order of magnitude above that of the Higgs.

Mass (GeV)	2.9	3.6	4.3	5.3	6.4
Selected Events	651(544)	1516(1324)	2048(2592)	947(2819)	116(1188)
Narrow Scan	455(460)	992(1144)	1656(2305)	860(2648)	107(1138)
CalRatio	337(261)	673(682)	876(1270)	345(1280)	30(407)
Overlap	241(222)	511(590)	734(1147)	316(1229)	29(399)
Final Events	570(499)	1154(1236)	1798(2428)	889(2699)	108(1146)

Table 6: Table displaying surviving number of events, out of 10000, for $pp \to Hjj$, $H \to \nu_i N_4$, $N_4 \to \nu_i \mu^+ \mu^-$ and $pp \to Zjj$, $Z \to \nu_i N_4$, $N_4 \to \nu_i \mu^+ \mu^-$(in parenthesis) after selection cuts and after different overlapping search regions. 2.9 GeV$< M_4 <$ 6.4 GeV at $|U_{\mu 4}|^2 = 10^{-6}$.

We observe that at M_4= 5.3 GeV the number of accepted events reaches a maximum. We show in Fig. 16 - 18 how the p_T of the electrons and the transverse decay distance of N_4 vary as the N_4 mass changes in a $H(Z) -> N_4\nu, N_4 -> \nu\mu^-\mu^+$ process.

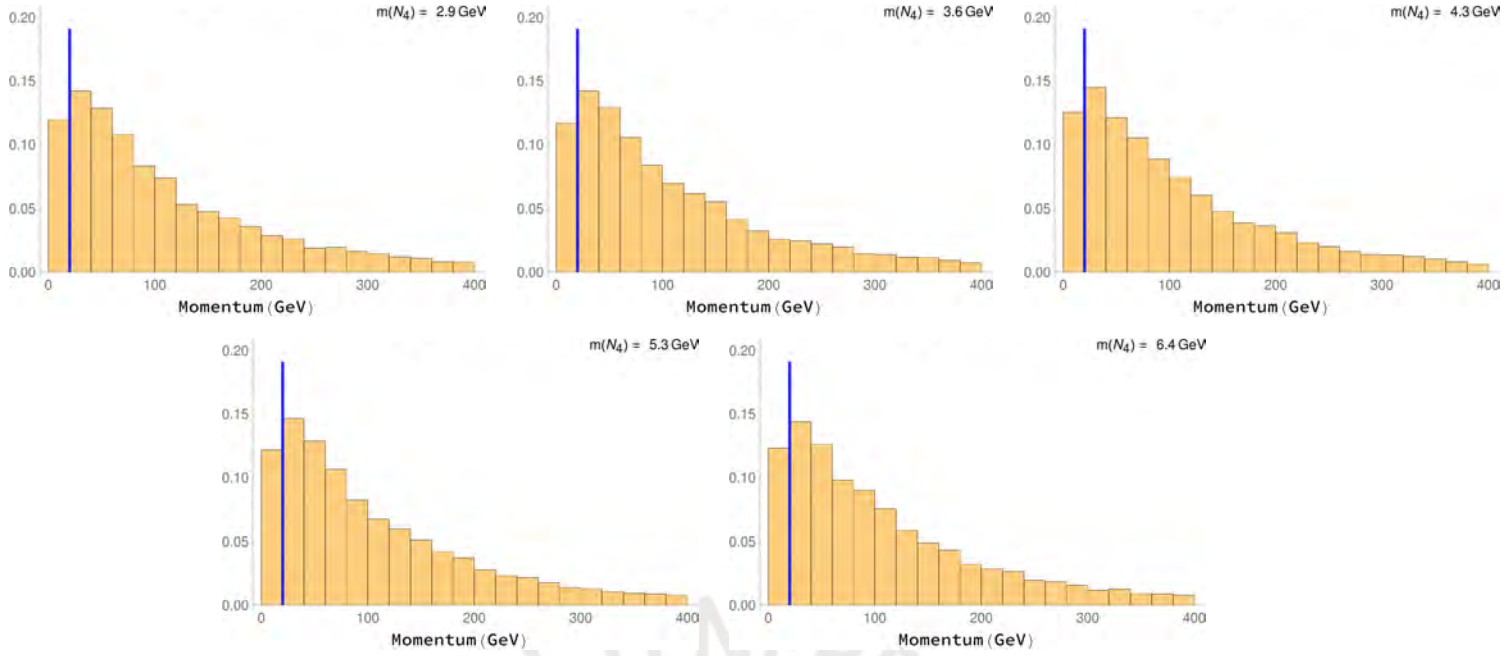

Figure 16: Normalized p_T distributions for highest μ component of lepton jet. Points right of the blue line at 20 GeV pass the Narrow Scan requirement.

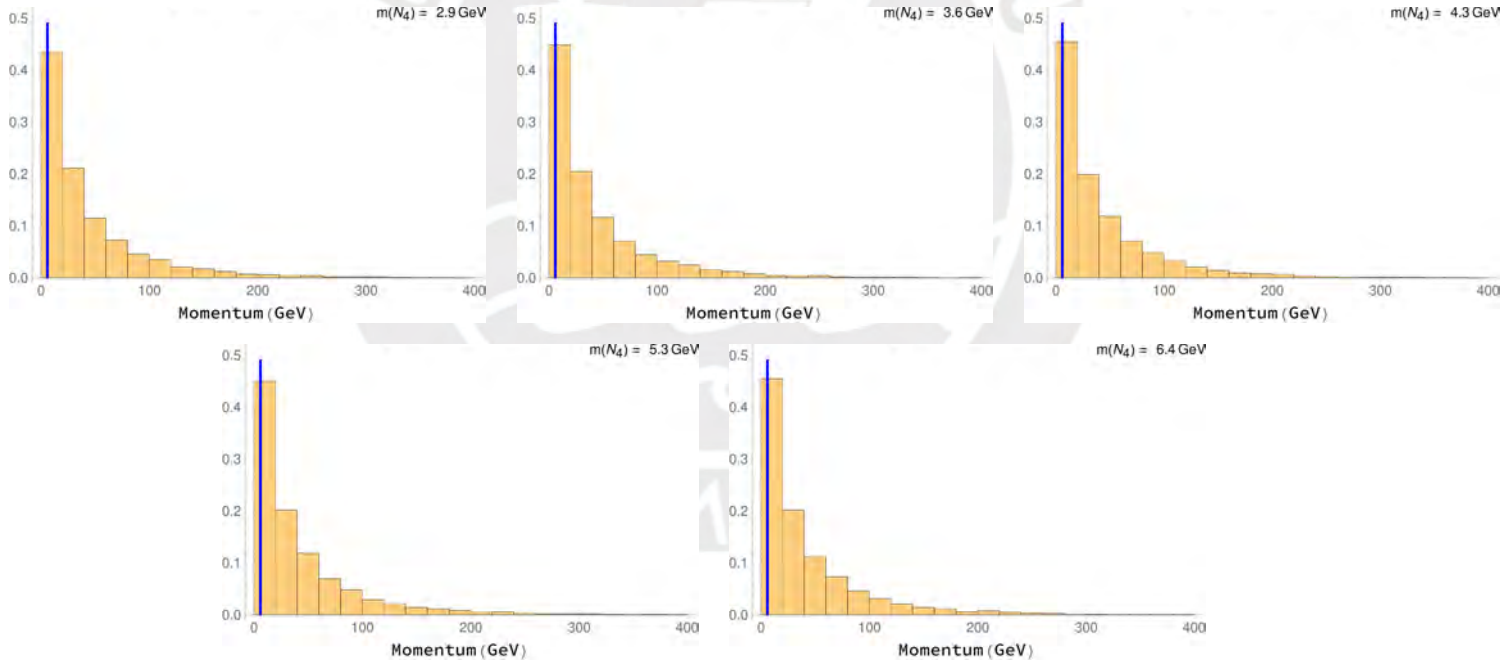

Figure 17: Normalized p_T distributions for second highest μ component of lepton jet. Points right of the blue line at 6 GeV pass the Narrow Scan requirement.

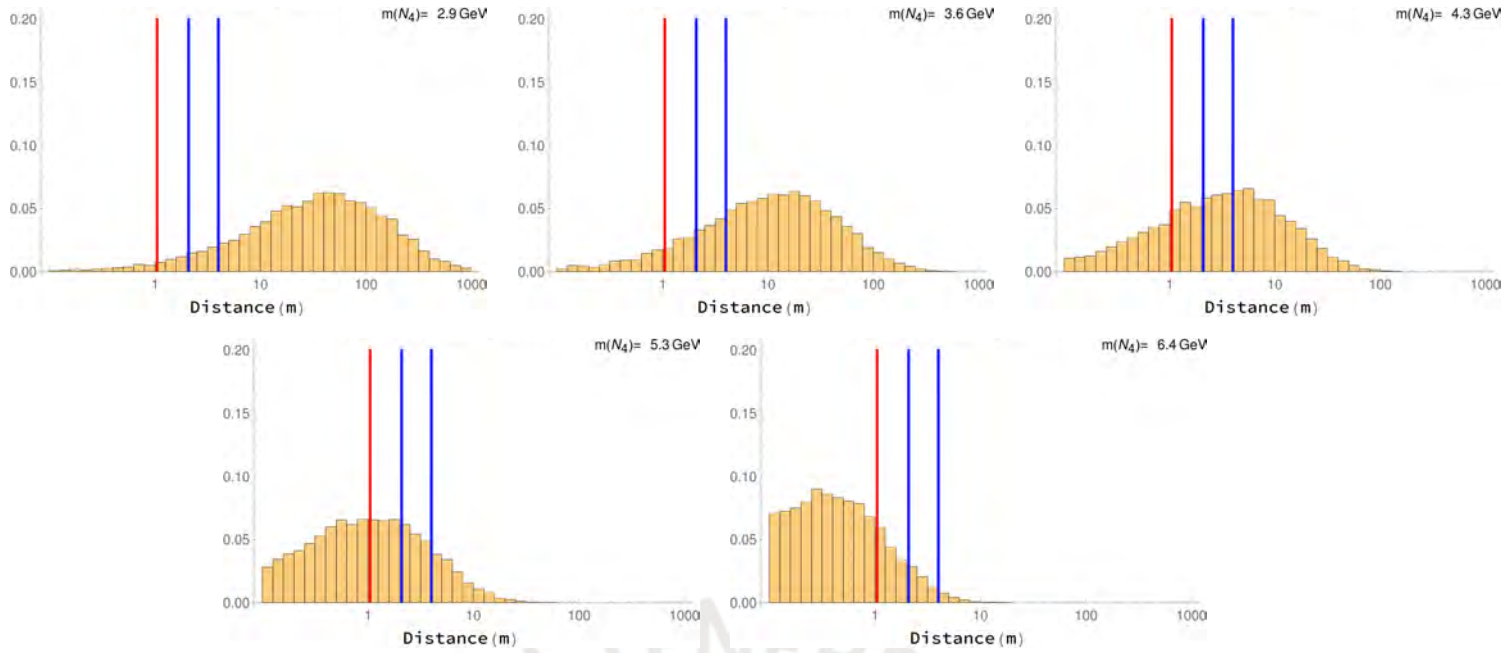

Figure 18: Normalized Transverse decay distances for N_4. Points right of the red line at 1.05m are non-combined. Those that fall between the blue lines (2.09 & 4 m) are in the range of the Hadronic Barrel calorimeter.

The blue line (Fig. 16) shows the minimum p_T for a Narrow Scan search. For the mass range displayed, most events pass the cut. The transverse decay distance (Fig. 18) decreases as the HN mass increases, which is expected. The red line shows the tracker radius, and the blue lines show the transverse range of the Hadronic Barrel. For Narrow Scan we consider decays inside either the Hadronic Barrel or the Hadronic Endcap (not displayed) In general, the heavy neutrino needs to decay in the region $\sqrt{L_x^2 + L_y^2} >$ 2.09 m, $|\eta| < 1.7$ for the Hadronic Barrel, and 1.05 m$< \sqrt{L_x^2 + L_y^2} <$ 2.09 m, $1.5 < |\eta| < 3.2$ for the Hadronic Endcap. The kinematics of the muons for M_4= 4.3 GeV, $|U_{\mu 4}|^2 = 10^{-6}$, chosen as the benchmark scenario, shows low p_T (Fig. 19) and ΔR (Fig. 20) distributions. The kinematical cuts in

this search favor these distributions (Table 7), thus, we see that these cuts are less stringent than a dilepton search. After all cuts, including weighted Higgs and Z boson contributions, around 2500 of the initial 10000 events survive. For the search regions:

- Narrow Scan: 2246 events
- CalRatio: 1234 events
- Overlap: 1110 events
- Final Events: 2370 events

After considering the cross-section and branching ratio for $\mu^-\mu^+$ production, an LHC(HL-LHC) search could expect 0.1 (1) events for the benchmark M_4= 4.3 GeV, $|U_{\mu 4}|^2 = 10^{-6}$, and 1(10) event for the scenario of highest mixing M_4= 3.6 GeV, $|U_{\mu 4}|^2 = 10^{-5}$.

The ATLAS documentation requires at least 2 lepton jets in their analysis. We have bypassed this requirement since we have additional selection criteria (VBF topology).

Cut Flow ($\mu\mu$)		
Criterion	Individual	Combined
$\|\eta(leptonjet)\| < 2.4$	9204	9204
$p_T(leptonjet) > 20GeV$	9091	8447
$\Delta R_{\mu\mu} < 0.5$	9471	8284
$\|z_o\|(\mu) < 280$ mm	7383	6361
$Non - combined$	3614	2552

Table 7: Table displaying individual and combined cuts for displaced lepton jets (Type 0) search simulation. Ten thousand initial events.

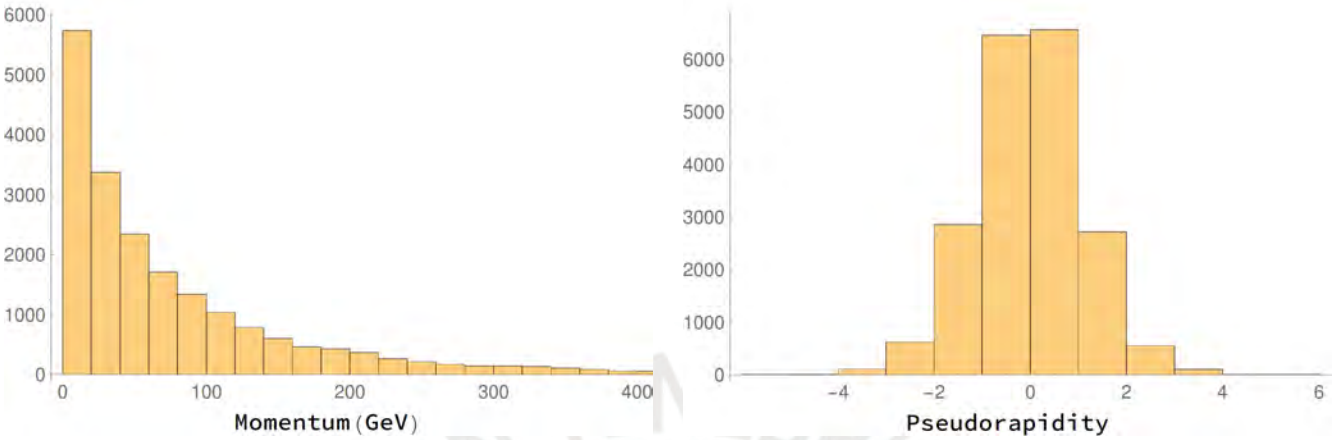

Figure 19: Left:Total p_T distribution for final state muons. Right:$|\eta|$ distribution for final state muons (Type 0).

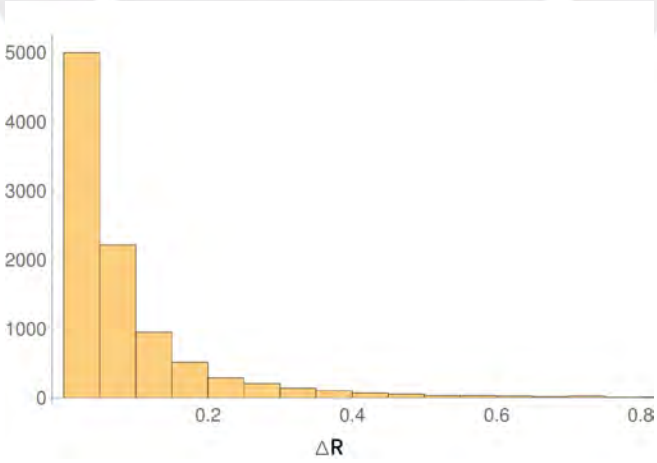

Figure 20: $\Delta R_{\mu\mu}$ distribution for final state muons (Type 0).

- Type 2($e^-e^+/e^\pm\pi^\mp$) search

We follow the cuts described in Chapter 4 that are available at simulation level. The additional calorimetry requirements presented by the ATLAS collaboration (Jet Timing, JVT, BIB), are not imposed. We generate, 10000 $pp \to H(Z)jj$, $H(Z) \to \nu_i N_4$, $N_4 \to \nu_i e^+e^-/e^\pm u^\mp d^\pm$ events. We maintain the squared mixing fixed ($|U_{\mu 4}|^2$= 10^{-6}), and analyze how the kinematics change for several neutrino masses In Table 8 we display the number of surviving events (out of 10000) for the selection cuts. Higgs and Z boson contributions are both considered. In this range $\frac{N_4 \to \nu_i e^\pm \pi^\mp}{N_4 \to \nu_i e^+ e^-} \simeq 3$, which is consistent with quarks having 3 colours.

Mass (GeV)	2.9	3.6	4.3	5.3	6.4
Total Events	341(319)	807(762)	1272(1322)	905(1129)	241(363)

Table 8: Table displaying surviving number of events, out of 10000, for $pp \to Hjj$, $H \to \nu_i N_4$, $N_4 \to \nu_i e^+e^-/e^\pm u^\mp d^\pm$ and $pp \to Zjj$, $Z \to \nu_i Z_4$, $Z_4 \to \nu_i e^+e^-/e^\pm u^\mp d^\pm$(in parenthesis) after Type 2 lepton jet selection cuts. 2.9 GeV$< M_4 <$ 6.4 GeV at $|U_{\mu 4}|^2$= 10^{-6}.

We observe that at M_4=4.3 GeV the number of accepted events reaches a maximum. For this scenario, we show in Fig. 21 - 23 how the p_T of the electrons and the transverse decay distance of the HN vary as the N_4 mass changes in a $H(Z) -> N_4\nu, N_4 -> \nu e^-/e^\pm\pi^\mp$ process.

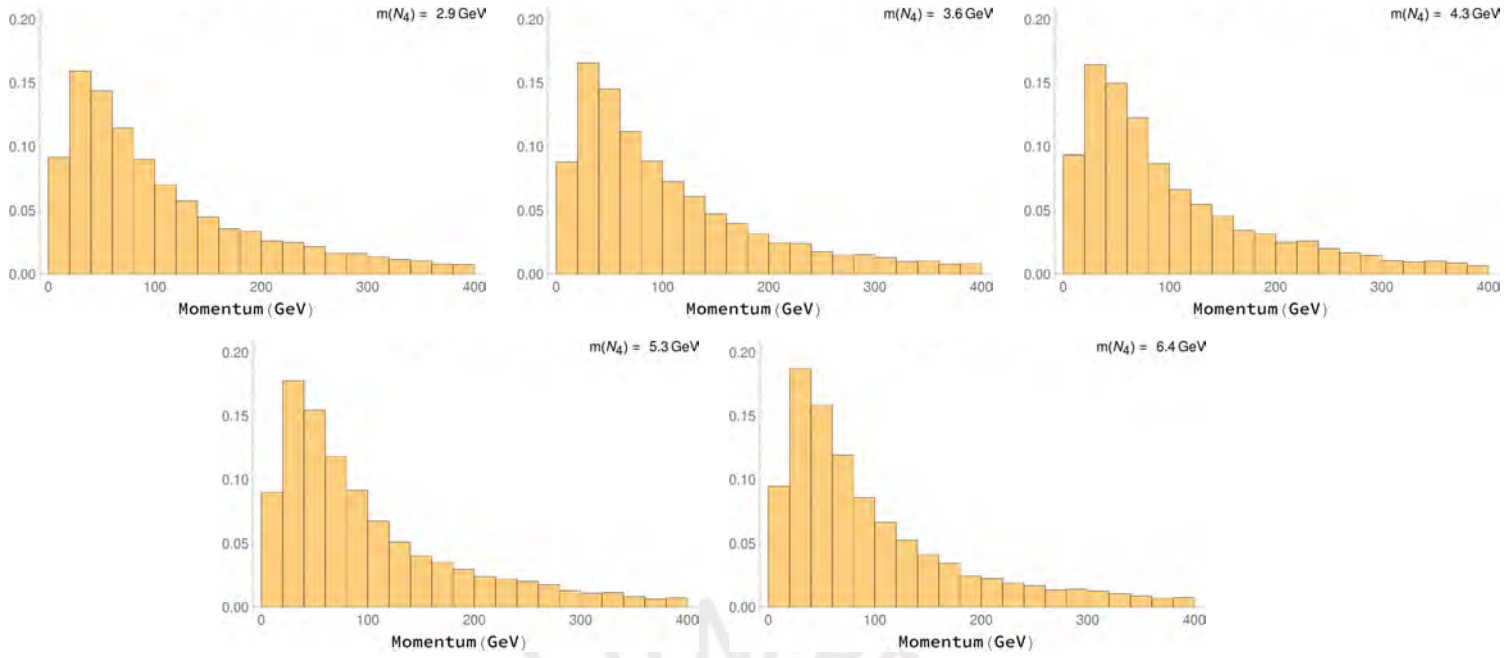

Figure 21: Normalized p_T distributions for highest component of lepton jet for Type 2 search.

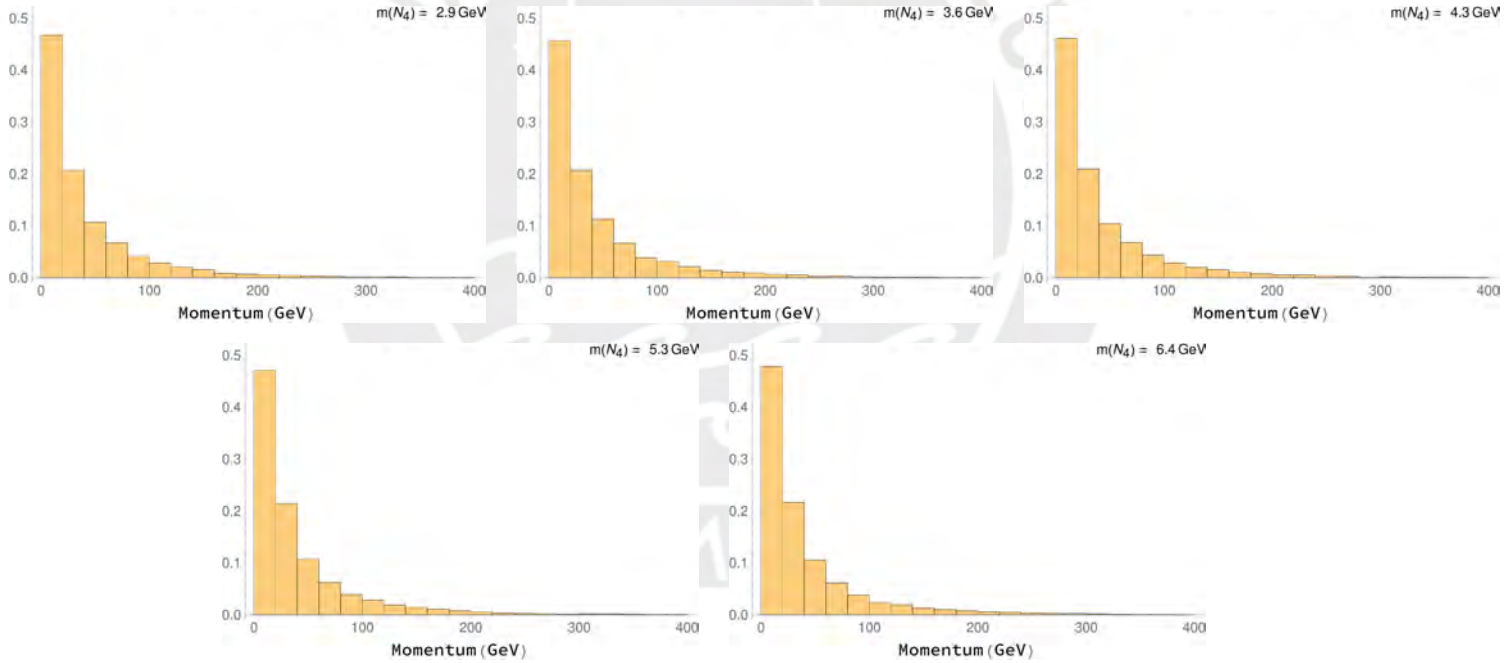

Figure 22: Normalized p_T distributions for second highest component of lepton jet for Type 2 search.

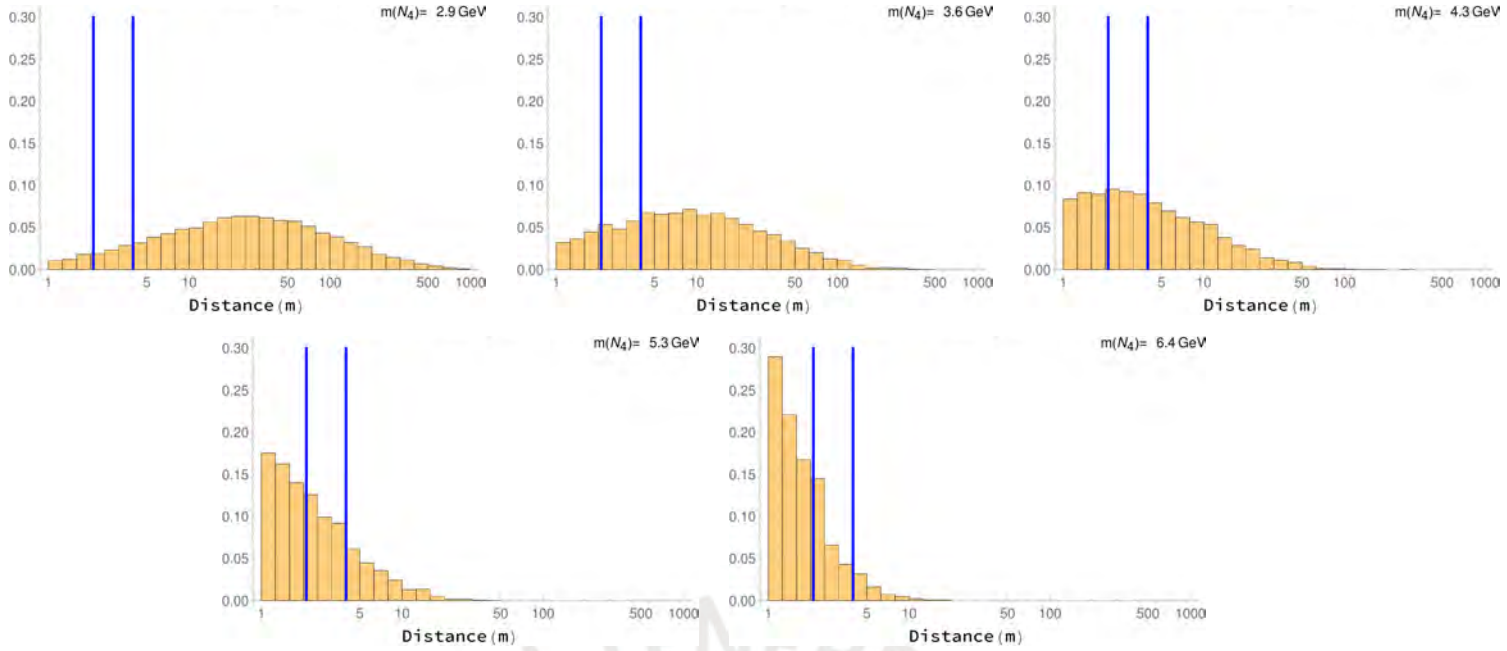

Figure 23: Normalized Transverse decay distances for N_4. Those that fall between the blue lines (2.09 & 4 m) are in the range of the Hadronic Barrel calorimeter

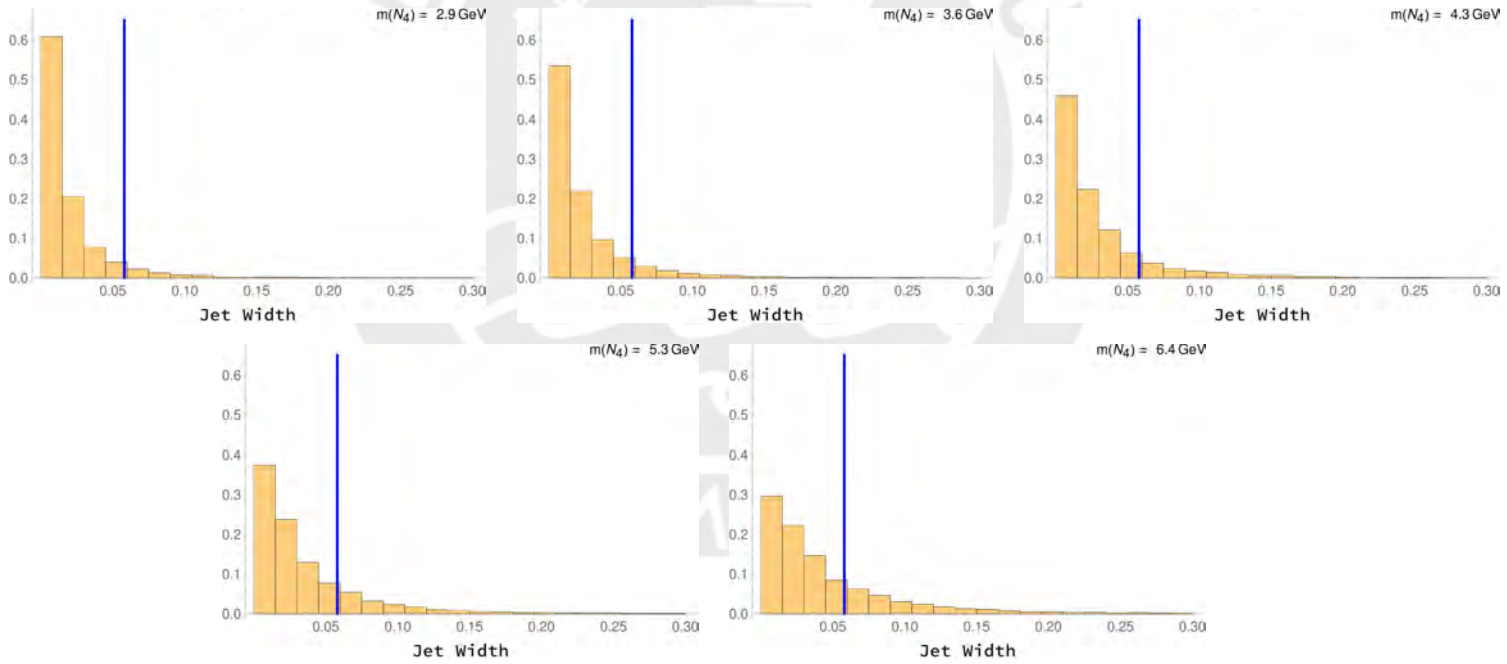

Figure 24: Normalized jet width for Type 2 lepton jet. Events to the left of the blue line pass the Jet Width cut.

The transverse decay distance (Fig. 23) decreases as the HN mass increases, which is expected. The blue lines show the transverse range of the Hadronic Barrel. We also consider decays inside the Hadronic Endcap.

The Jet Width (Fig. 24) increases with M_4. Events to the left of the blue line at 0.058 pass the Jet Width cut. The kinematics of the electron for the benchmark scenario show low p_T (Fig. 25) and ΔR (Fig. 26) distributions. The kinematical cuts in this search favor these distributions (Table 9), thus, we see that these cuts are less stringent than a dilepton search. This is present in both lepton jet analysis. After all cuts, and weighting Higgs and Z boson contributions, around 1200 of the initial 10000 survive. After considering cross-sections and branching ratios, an LHC(HL-LHC) search could expect 0.2(2) events for the benchmark $M_4 = 4.3$ GeV, $|U_{\mu 4}|^2 = 10^{-6}$, or 2(20) events for the scenario of highest mixing $M_4 = 3.6$ GeV, $|U_{\mu 4}|^2 = 10^{-5}$.

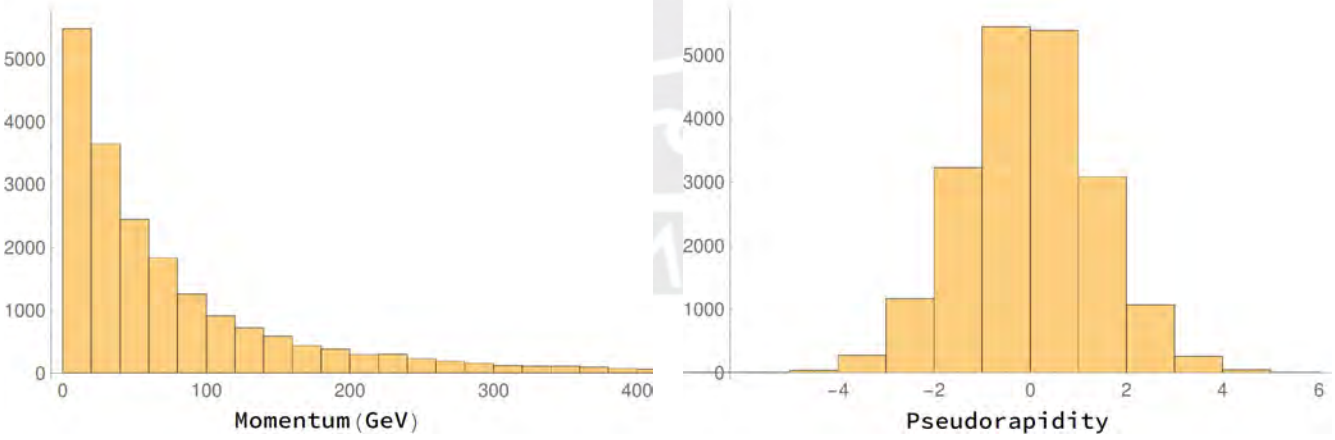

Figure 25: Left:Total p_T distribution for final state jet constituents. Right:$|\eta|$ distribution for final state jet constituents.

A lepton jet search at the HL-LHC could yield around 3 events at 3000 fb^{-1} integrated Luminosity for the bench mark, and up to 30 events in a best case scenario.

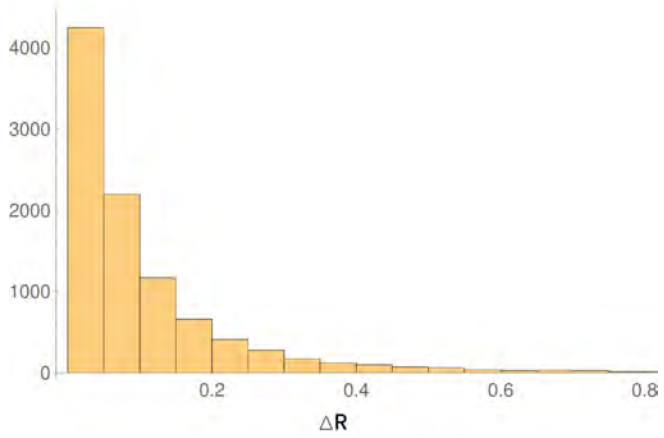

Figure 26: ΔR_{ee} distribution for final state jet constituents.

Cut Flow (ee)		
Criterion	Individual	Combined
$\lvert\eta(leptonjet)\rvert < 2.4$	7129	7129
$p_T(leptonjet) > 20GeV$	9415	6773
$\Delta R_{ee} < 0.5$	9411	6567
$JetWidth < 0.058$	8455	6017
Low $EM\ Fraction$	2198	1295

Table 9: Table displaying individual and combined cuts for displaced lepton jets (Type 2) search simulation. Ten thousand initial events.

5.3 Displaced Jet Searches

The cuts displayed in Chapter 4 for Displaced Jets are considerably stringent, and make the search unviable for this model. This is particularly true for the p_T^{miss} requirements.

The missing p_T distribution is shown in Fig. 27. Less than 20 and 5 percent of the events survive the p_T^{miss} cuts, for CMS and ATLAS respectively.

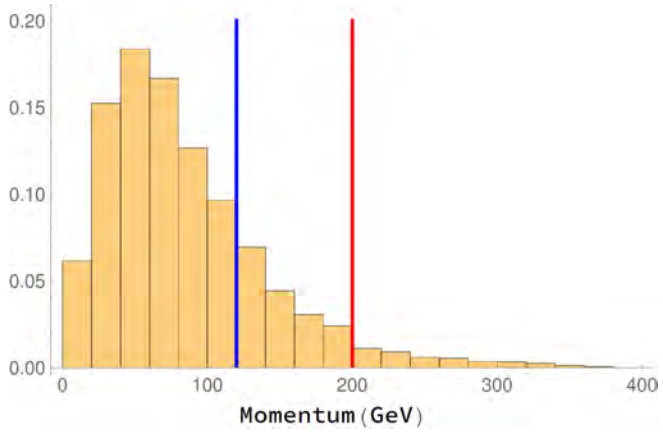

Figure 27: Missing p_T for the benchmark M_4= 14 GeV, $|U_{\mu 4}|^2$= 10^{-6}. Events to the right of the blue(red) line pass the CMS(ATLAS) p_T^{miss} requirement.

6 Conclusions

We studied the possible detection of heavy neutrinos involved in VBF processes, via displaced vertex in the LHC. We have based our study on a 3+3 Seesaw type I model with heavy neutrino masses in the GeV scale. We have two almost degenerate heavy Majorana neutrinos ($M_{4,5} \simeq 1 - 50$ GeV) with considerable mixings to the SM, ($|U_{\mu 4}|^2 \simeq 10^{-7} - 10^{-5}$), and a heaviest third ($M_6 = 100$GeV) decoupled from the theory. This model then behaves like an effective 3+2. The parameters in the model are tuned in such a way that heavy neutrino masses are generated below the electroweak scale without the need of excessively large mixings.

The model is implemented in SPheno for the parameter space of interest. Proton proton collisions are simulated in MadGraph, with model input from SPheno to obtain N_4 events from the decay of the Higgs and Z boson. Cross Sections

for $pp \to H(Z)jj, H(Z) \to N_4\nu_\mu$ range from 10^{-4} to 10^{-6} pb. Both channels have the same dependence on $|U_{\mu 4}|^2$, but Z channel depends on M_4 only kinematically. The posterior decays and hadronization are ran in Pythia8, and the truth level information is stored in HEPMC format. In the section of the parameter space interesting for displaced vertices ($L_{N_4} \simeq 1mm - 1m$) relatively low M_4 masses are required, and in this mass range Z boson contributions an order of magnitude above those of the Higgs. The anticipated number of events at the LHC ($\sqrt{s} = 13$ TeV and L =300 fb$^-1$) is around 30 events in a best case scenario (M_4= 3.6 GeV, $|U_{\mu 4}|^2$= 10^{-5}), without any consideration of detector efficiencies, which is subject of a future work [22]. Future expectations for the HL-LHC ($\sqrt{s} = 14$ TeV and L =3000 fb$^-1$) could improve the search by and order of magnitude, which may be necessary to observe these events.

We study three possible N_4 decay channels that could allow for heavy neutrino detection:

- Displaced Dileptons with a e and μ pair, which requires high p_T and a large ΔR separation between leptons. Not feasible for single neutrino production even in the HL-LHC, since a boosted pair of leptons tend to be collimated. This type of search might work in models with more than 1 heavy neutrino as decay product.

- Lepton jets, which are leptons or pions inside a cone of $\Delta R < 0.4$. We

expect to overcome the requirement of having at least 2 lepton jets with the VBF topology. The search has opposite requirements to those of displaced leptons: low ΔR distances and considerably low minimunum p_T, which makes it ideal in this scenario. Via this search, the model expects up to 3 events per HL-LHC run in the case of $|U_{\mu 4}|^2 = 10^{-6}$. If one goes to the current bound $|U_{\mu 4}|^2 = 10^{-5}$ around 38 events could be expected.

- Displaced jets which require jets generated away from the primary vertex, are studied, but a search is not implemented and is left as subject of a posterior work.

A HEPMC data extraction and processing

HepMC is an object oriented event record written in C++ for Monte Carlo Generators in High Energy Physics [37]. It serves as an output format for the event information, from the main vertex collision to the decay products and posterior hadronization. It contains the information (4-momentum, id, mass, parent vertex, etc.) of every particle and vertex in the event. The information is at truth level, not as reconstructed by the detector. Using Root we extract the energy and momentum of the heavy neutrino and its decay products. From this we construct in Mathematica the quantities used in the analysis, such as pseudora-

pidity η and transverse momentum p_T. The neutrino average lifetime in the lab frame is constructed as:

$$\tau = \frac{E_{N_4}}{M_{N_4}} \cdot \frac{\hbar}{\Gamma_o} = \gamma \frac{\hbar}{\Gamma_o} \tag{29}$$

in seconds, where Γ_0 is calculated at rest.

The actual lifetime follows an inverse exponential distribution:

$$\exp\left[-\frac{t}{\tau}\right], \quad t > 0 \tag{30}$$

According to this distribution we randomly generate the decay length as:

$$\vec{l} = \frac{\vec{p}_{N_4}}{E_{N_4}} \cdot c \cdot t. \tag{31}$$

References

[1] K. Eguchi et al. "First results from KamLAND: Evidence for reactor anti-neutrino disappearance". In: *Phys. Rev. Lett.* 90 (2003), p. 021802. DOI: 10.1103/PhysRevLett.90.021802. arXiv: hep-ex/0212021 [hep-ex].

[2] Q. R. Ahmad et al. "Direct evidence for neutrino flavor transformation from neutral current interactions in the Sudbury Neutrino Observatory". In: *Phys. Rev. Lett.* 89 (2002), p. 011301. DOI: 10.1103/PhysRevLett.89.011301. arXiv: nucl-ex/0204008 [nucl-ex].

[3] Y. Fukuda et al. “Measurement of the flux and zenith angle distribution of upward through going muons by Super-Kamiokande”. In: *Phys. Rev. Lett.* 82 (1999), pp. 2644–2648. DOI: 10.1103/PhysRevLett.82.2644. arXiv: hep-ex/9812014 [hep-ex].

[4] Peter Minkowski. “$\mu \to e\gamma$ at a rate of one out of 109 muon decays?” In: *Physics Letters B* 67 (Apr. 1977), pp. 421–428. DOI: 10.1016/0370-2693(77)90435-X.

[5] Murray Gell-Mann, Pierre Ramond, and Richard Slansky. “Complex Spinors and Unified Theories”. In: *Conf. Proc.* C790927 (1979), pp. 315–321. arXiv: 1306.4669 [hep-th].

[6] Rabindra N. Mohapatra. “Neutrino Mass and Spontaneous Parity Nonconservation”. In: *Phys. Rev. Lett.* 44 (14 1980), pp. 912–915. DOI: 10.1103/PhysRevLett.44.912. URL: https://link.aps.org/doi/10.1103/PhysRevLett.44.912.

[7] Tsutomu Yanagida. “Horizontal gauge symmetry and masses of neutrinos”. In: *Conf. Proc.* C7902131 (1979), pp. 95–99.

[8] K. N. Abazajian et al. “Light Sterile Neutrinos: A White Paper”. In: (2012). arXiv: 1204.5379 [hep-ph].

[9] P. Hernández, J. Jones-Pérez, and O. Suarez-Navarro. “Majorana vs Pseudo-Dirac Neutrinos at the ILC”. In: *Eur. Phys. J.* C79.3 (2019), p. 220. DOI: 10.1140/epjc/s10052-019-6728-1. arXiv: 1810.07210 [hep-ph].

[10] A. Donini et al. “The minimal 3+2 neutrino model versus oscillation anomalies”. In: *JHEP* 07 (2012), p. 161. DOI: 10.1007/JHEP07(2012)161. arXiv: 1205.5230 [hep-ph].

[11] Alberto M. Gago et al. “Probing the Type I Seesaw Mechanism with Displaced Vertices at the LHC”. In: *Eur. Phys. J.* C75.10 (2015), p. 470. DOI: 10.1140/epjc/s10052-015-3693-1. arXiv: 1505.05880 [hep-ph].

[12] R. Alonso et al. “Muon conversion to electron in nuclei in type-I seesaw models”. In: *JHEP* 01 (2013), p. 118. DOI: 10.1007/JHEP01(2013)118. arXiv: 1209.2679 [hep-ph].

[13] F. Staub. “SARAH”. In: (2008). arXiv: 0806.0538 [hep-ph].

[14] W. Porod and F. Staub. “SPheno 3.1: Extensions including flavour, CP-phases and models beyond the MSSM”. In: *Comput. Phys. Commun.* 183 (2012), pp. 2458–2469. DOI: 10.1016/j.cpc.2012.05.021. arXiv: 1104.1573 [hep-ph].

[15] Werner Porod. "SPheno, a program for calculating supersymmetric spectra, SUSY particle decays and SUSY particle production at e+ e- colliders". In: *Comput. Phys. Commun.* 153 (2003), pp. 275–315. DOI: 10.1016/S0010-4655(03)00222-4. arXiv: hep-ph/0301101 [hep-ph].

[16] Georges Aad et al. "Observation of a new particle in the search for the Standard Model Higgs boson with the ATLAS detector at the LHC". In: *Phys. Lett.* B716 (2012), pp. 1–29. DOI: 10.1016/j.physletb.2012.08.020. arXiv: 1207.7214 [hep-ex].

[17] Serguei Chatrchyan et al. "Observation of a New Boson at a Mass of 125 GeV with the CMS Experiment at the LHC". In: *Phys. Lett.* B716 (2012), pp. 30–61. DOI: 10.1016/j.physletb.2012.08.021. arXiv: 1207.7235 [hep-ex].

[18] Matthew D. Schwartz. "TASI Lectures on Collider Physics". In: *Proceedings, Theoretical Advanced Study Institute in Elementary Particle Physics : Anticipating the Next Discoveries in Particle Physics (TASI 2016): Boulder, CO, USA, June 6-July 1, 2016*. 2018, pp. 65–100. DOI: 10.1142/9789813233348_0002. arXiv: 1709.04533 [hep-ph].

[19] Abdelhak Djouadi. "The Anatomy of electro-weak symmetry breaking. I: The Higgs boson in the standard model". In: *Phys. Rept.* 457 (2008), pp. 1–216. DOI: 10.1016/j.physrep.2007.10.004. arXiv: hep-ph/0503172 [hep-ph].

[20] Andrés Flórez et al. "Searching for New Heavy Neutral Gauge Bosons using Vector Boson Fusion Processes at the LHC". In: *Phys. Lett.* B767 (2017), pp. 126–132. DOI: 10.1016/j.physletb.2017.01.062. arXiv: 1609.09765 [hep-ph].

[21] Andrés Flórez et al. "Expanding the Reach of Heavy Neutrino Searches at the LHC". In: *Phys. Lett.* B778 (2018), pp. 94–100. DOI: 10.1016/j.physletb.2018.01.009. arXiv: 1708.03007 [hep-ph].

[22] J. Jones-Pérez, J. Masias, and J. Ruiz. In preparation. In: ().

[23] Asmaa Abada et al. "Inclusive Displaced Vertex Searches for Heavy Neutral Leptons at the LHC". In: *JHEP* 01 (2019), p. 093. DOI: 10.1007/JHEP01(2019)093. arXiv: 1807.10024 [hep-ph].

[24] Marco Drewes and Jan Hajer. "Heavy Neutrinos in displaced vertex searches at the LHC and HL-LHC". In: (2019). arXiv: 1903.06100 [hep-ph].

[25] J. Alwall et al. “The automated computation of tree-level and next-to-leading order differential cross sections, and their matching to parton shower simulations”. In: *JHEP* 07 (2014), p. 079. DOI: 10.1007/JHEP07(2014)079. arXiv: 1405.0301 [hep-ph].

[26] Torbjorn Sjostrand, Stephen Mrenna, and Peter Z. Skands. “A Brief Introduction to PYTHIA 8.1”. In: *Comput. Phys. Commun.* 178 (2008), pp. 852–867. DOI: 10.1016/j.cpc.2008.01.036. arXiv: 0710.3820 [hep-ph].

[27] Torbjorn Sjostrand, Stephen Mrenna, and Peter Z. Skands. “PYTHIA 6.4 Physics and Manual”. In: *JHEP* 05 (2006), p. 026. DOI: 10.1088/1126-6708/2006/05/026. arXiv: hep-ph/0603175 [hep-ph].

[28] Florian Staub et al. “A Tool Box for Implementing Supersymmetric Models”. In: *Comput. Phys. Commun.* 183 (2012), pp. 2165–2206. DOI: 10.1016/j.cpc.2012.04.013. arXiv: 1109.5147 [hep-ph].

[29] G. Bélanger et al. “LHC-friendly minimal freeze-in models”. In: *JHEP* 02 (2019), p. 186. DOI: 10.1007/JHEP02(2019)186. arXiv: 1811.05478 [hep-ph].

[30] Vardan Khachatryan et al. “Search for Displaced Supersymmetry in events with an electron and a muon with large impact parameters”. In: *Phys. Rev. Lett.* 114.6 (2015), p. 061801. DOI: 10.1103/PhysRevLett.114.061801. arXiv: 1409.4789 [hep-ex].

[31] CMS Collaboration. “Search for displaced leptons in the e-mu channel”. In: (2016).

[32] The ATLAS collaboration. “Search for long-lived neutral particles decaying into displaced lepton jets in proton–proton collisions at $\sqrt{s}$ = 13 TeV with the ATLAS detector”. In: (2016).

[33] Georges Aad et al. “Search for long-lived neutral particles decaying into lepton jets in proton-proton collisions at $\sqrt{s} = 8$ TeV with the ATLAS detector”. In: *JHEP* 11 (2014), p. 088. DOI: 10.1007/JHEP11(2014)088. arXiv: 1409.0746 [hep-ex].

[34] G. Aad et al. “Expected Performance of the ATLAS Experiment - Detector, Trigger and Physics”. In: (2009). arXiv: 0901.0512 [hep-ex].

[35] CMS Collaboration. “Search for long-lived particles using delayed jets and missing transverse momentum with proton-proton collisions at $\sqrt{s}$ = 13 TeV”. In: (2019).

[36] Morad Aaboud et al. “Search for long-lived, massive particles in events with displaced vertices and missing transverse momentum in $\sqrt{s}$ = 13 TeV pp collisions with the ATLAS detector”. In: *Phys. Rev.* D97.5 (2018), p. 052012. DOI: 10.1103/PhysRevD.97.052012. arXiv: 1710.04901 [hep-ex].

[37] Matt Dobbs and Jørgen Beck Hansen. “The HepMC C++ Monte Carlo event record for High Energy Physics”. In: *Computer Physics Communications* 134 (Jan. 2001). DOI: 10.1016/S0010-4655(00)00189-2.